TOPICAL REVIEW — Amorphous physics and materials

# Multiscale structures and phase transitions in metallic glasses: A scattering perspective*

Si Lan(兰司)[1,2,†], Zhenduo Wu(吴桢舵)[1,3,†], and Xun-Li Wang(王循理)[1,3,‡]

[1] Department of Physics and Materials Science, City University of Hong Kong, Kowloon, Hong Kong, China
[2] Herbert Gleiter Institute of Nanoscience, Nanjing University of Science and Technology, Nanjing 210094, China
[3] City University of Hong Kong Shenzhen Research Institute, Shenzhen 518057, China

(Received 29 November 2016; revised manuscript received 23 December 2016; published online 29 December 2016)

Amorphous materials are ubiquitous and widely used in human society, yet their structures are far from being fully understood. Metallic glasses, a new class of amorphous materials, have attracted a great deal of interests due to their exceptional properties. In recent years, our understanding of metallic glasses increases dramatically, thanks to the development of advanced instrumentation, such as *in situ* x-ray and neutron scattering. In this article, we provide a brief review of recent progress in study of the structure of metallic glasses. In particular, we will emphasize, from the scattering perspective, the multiscale structures of metallic glasses, i.e., short-to-medium range atomic packing, and phase transitions in the supercooled liquid region, e.g., crystallization and liquid-to-liquid phase transition. We will also discuss, based on the understanding of their structures and phase stability, the mechanical and magnetic properties of metallic glasses.

**Keywords:** metallic glasses, phase transitions, neutron scattering, x-ray scattering

**PACS:** 71.23.Cq, 64.70.–p, 61.05.F–, 61.05.cf **DOI:** 10.1088/1674-1056/26/1/017104

## 1. Introduction

Metallic glasses (MGs) constitute a new class of metallic materials with unique properties, including high strength, high elastic limit, high wear and corrosion resistance, and excellent soft magnetic behavior, for structural and functional applications.[1,2] MGs can be formed when a liquid is frozen very quickly. The liquid–glass (LG) transition is thus featured with drastic slowing down of relaxation time (increasing of viscosity) upon cooling. L–G transition is considered as the consequence of the cooperative development of short-range ordering (SRO) and medium-range ordering (MRO),[3] which have incompatible local symmetry compared to the long-range density ordering toward crystallization. The L–G transition is thus a process accompanied not only by structure change but also by dynamic evolution. The physical origin of L–G transition has been one of the most challenging, unresolved issues in condense matter physics.[4–6] Studying the atomic packing schemes of liquid and glassy states for MGs (Section 2) may be one way to begin unraveling the issues associated with the physical origin of the L–G transition. Examining the hidden role of crystallization on vitrification helps to further understanding of the L–G transition and glass-forming ability (GFA) (Section 3). Investigating the liquid–liquid phase transition (LLPT) (Section 4), which may be a general phenomenon in all liquids capable of forming locally favored structures (LFS) upon cooling, may also provide means of explaining the slow dynamics and the origin of fragility and its related fragile-to-strong (F–S) transition. Based on the understanding of the above portions of this paper, we may be able to cast additional light on the mechanical property (Section 5) and soft-magnetic property of MGs (Section 6).

As cutting-edge techniques, scattering techniques, including neutron and high-energy synchrotron x-ray scattering, are very convenient for *in situ* study of the structure and dynamics of both liquids and glass under different experimental conditions, such as pressure- or temperature-dependent experiments. Non-destructive, high-penetration scattering experiments equipped with large area 2D detectors can probe structure information in reciprocal space over a wide momentum transfer $Q$ ($Q = 4\pi \sin\theta/\lambda$). Here $\theta$ is half of the scattering angle between the incident beam and the scattered beam, and $\lambda$ is the neutron or x-ray wavelength. The reduced pair distribution function (PDF), $G(r)$, is obtained from the Fourier transform of structure factor $S(Q)$: $G(r) = (2/\pi) \times \int_0 Q_{\max} Q\,(S(Q) - 1) \sin(Qr)\,\mathrm{d}Q$, where $r$ is the atomic distance in real space. So the scattering experiment results

*Project supported by Shenzhen Science and Technology Innovation Commission of China (Grant No. R-IND8701) and the Croucher Foundation (Project No. CityU 9500020). Si Lan is partially supported by the Fundamental Research Funds for the Central Universities of China (Grant No. 30915015103) and the National Natural Science Foundation of China (Grant No. 51501090). Zhenduo Wu and Xun-Li Wang are partially supported by the National Natural Science Foundation of China (Grant No. 51571170).

†These two authors contributed equally.
‡Corresponding author. E-mail: xlwang@cityu.edu.hk

© 2017 Chinese Physical Society and IOP Publishing Ltd 

can provide unique structural information of materials, from atomic to nanometer scale.[7,8] This review paper highlights the scattering perspectives of structure- (Sections 2–4) and properties- (Sections 5 and 6) related issues of MGs in recent years and may provide insights on structure–property correlations of MGs from the perspectives of scattering science and technologies.

## 2. Atomic packing in metallic glass

Atomic packing has been a long-standing issue for amorphous solids, liquids, and soft matters. Unlike crystalline materials, disordered materials do not have periodic unit cells that can perfectly fill in three-dimensional space and pack to achieve long-range ordering. The most efficient atomic packing configurations in crystalline materials are the face-centered cubic (FCC) and the hexagonal closest packed (HCP). Metallic glass (MG) can be formed by quenching molten liquid from a high temperature to room temperature. Although free volumes can be cast from loose packing liquid into dense packing glass, the packing coefficient for MGs is still close to that of their crystalline counterparts.[9] Bernal's dense random hard-sphere packing model[10,11] was proposed about a half-century ago and has been widely cited for monoatomic liquid or glass. However, it fails to describe the atomic arrangement of MGs that have more than two components; these have been found to have a pronounced topological/chemical short-range order (SRO).[12–14] The global packing scheme for MGs remains mysterious.

The studies of atomic packing from the short-to-medium range can aid in understanding GFA and the properties of MGs. As shown in Fig. 1(a), the atomic structural model for MGs has been proposed by Miracle *et al.*[15] This model is based on solute-centered clusters plus the FCC or HCP sphere-packing scheme. As shown in Fig. 1(b), solute-centered clusters are considered a sphere-like structure element and the structure extended to medium range can be produced by packing the spheres in whole space in the scheme of FCC or HCP. Solvent atoms can be shared by clusters in faces, edges, or vertices. This model can fit the experimental pair distribution function (PDF) very well. This packing scheme is reasonable because the solute-solvent bonds prefer to form as a result of their large negative heat of mixing.[1] This structure model was successfully deployed to fit the PDFs for multicomponent system BAM 11 ($Zr_{52.5}Cu_{17.9}Ni_{14.6}Al_{10}Ti_5$) by Ma *et al.*,[16] which was treated as a pseudo-ternary alloy system. As shown in Fig. 1(c), solute-center polyhedra, such as Icosahedra, have been proven to be candidate local packing units for achieving dense packing[13,17] for MGs. Different alloy systems may form different polyhedra based on the effective atomic size ratio between solute and solvent atoms. However, this polyhedron cannot perfectly tile in the whole space in a scheme of FCC, HCP, or icosahedral order without involving distortion or defects.[18,19] As illustrated in Fig. 1(d), defects, such as 'vacancies' and even 'cavities', may frequently form amongst multiple solute-centered clusters for MGs. As shown in Figs. 1(e) and 1(f), the degree of connectivity for Zr–Cu MG can be greatly enhanced by the addition of elements such as Al that can optimize the atomic ratio between solute and solvent atoms to form full icosahedra.[20]

Recently, fractal packing schemes at medium-range scale have been experimentally observed in 37 MGs by Ma *et al.*,[21] which show a higher packing efficient than that of cubic packing and icosahedral order packing as demonstrated by simulations. Compared to cubic packing, fractal means self-similarity and scale invariance, and this has been clearly demonstrated in a variety of systems including polymers, colloids, and nanoparticles in suspension, etc.[22] The primary evidence for fractal packing, as shown in Fig. 1(g), is the power law scaling of the position of the first sharp diffraction peak (FSDP) $Q_1$ in a powder diffraction pattern with atomic volume $v_a$. A power of 1/3 can always be identified for crystalline materials such as FCC copper. However, a power of 0.433 was determined for many MGs. The corresponding fractal dimension $D_f$ is 2.31. As shown in Fig. 1(h), using *in situ* high-pressure x-ray diffraction (XRD) and *in situ* density measuring techniques, including ultrasonic sound velocity and full field nanoscale x-ray transmission microscopy (TXM), Zeng *et al.*[23] later observed that the density of a compressible MG, $La_{62}Al_{14}Cu_{11.7}Ag_{2.3}Ni_5Co_5$, has 2.5 power of $Q_1$ instead of a cubic relationship.

An early MD simulation study by Barmin *et al.*[24] analyzed the atomic structure of pure amorphous Re and Re–Tb amorphous alloys in the framework of percolation theory, and demonstrated that the dense areas in the amorphous matrix form the fractal skeleton. Later, Chen *et al.*[25] proposed a dimensionality crossover between fractal short-range ($D_f = \sim 2.5$) and homogeneous long-range structures ($D_f = \sim 3$) using *in situ* x-ray diffraction, tomography, and molecular dynamic (MD) simulations. The percolation theory was used to determine the correlation length for fractal packing, which was proposed to be limited to the first and second coordination shells. Beyond the scaling analysis of $Q_1$, Ma *et al.*[21] also clearly demonstrated the correlation between FSDP $Q_1$ and MRO from 6 Å to 20 Å by using Fourier transforming different peaks in experimental scattering structure factor $S(Q)$ to obtain reduced PDF $G(r)$. Thus, the fractal dimension in Ma's paper can be applied to the packing scheme of MGs at medium-range scale, which is related to the inter-atomic distance beyond the nearest neighbors.

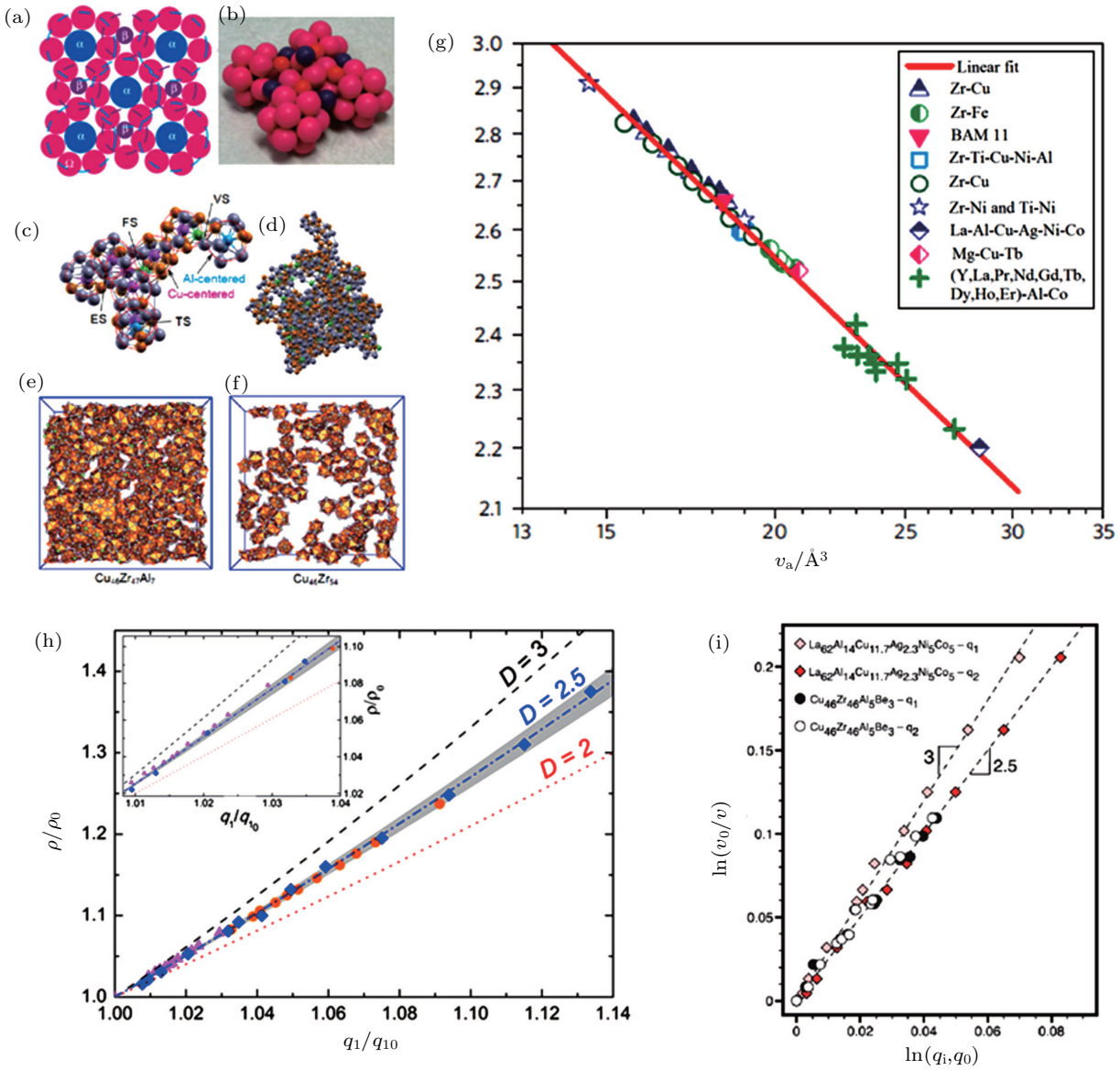



**Fig. 1.** (color online) Atomic packing of metallic glasses. (a) and (b) Solute-centered clusters plus FCC or HCP sphere-packing scheme proposed by Miracle.[15] With permission from Nature Materials. Copyright 2004 Nature Publishing Group. Solute-centered clusters are considered as the sphere-like structure element. Different colors represent solvent or solute atoms with different atomic size. (c) Solute-center polyhedra, such as Icosahedra, as the structure units and connected by sharing vertex (VS), faces (FS), tetrahedra (TS), and edges (ES).[20] (d) The existence of defects, such as 'vacancies' even 'cavities' in MGs.[20] With permission from Physical Review Letters. Copyright 2009 American Physics Society. The illustration of the connectivity degree of the full icosahedra in (e) $Cu_{46}Zr_{47}A_{l7}$ MG and (f) $Cu_{46}Zr_{54}$ MG. (g) Power-law scaling and fractal nature of metallic glasses revealed by the statistics of the relationship between $Q_1$ and density of a variety of MGs.[21] With permission from Nature Materials. Copyright 2009 Nature Publishing Group. (h) The density of a compressible MG, $La_{62}Al_{14}Cu_{11.7}Ag_{2.3}Ni_5Co_5$, has 2.5 power of $Q_1$.[23] With permission from Physical Review Letters. Copyright 2014 American Physics Society. (I) A dimensionality crossover between fractal short-range ($D_f = \sim 2.5$) and homogeneous long-range structures ($D_f = 3$).[25] With permission from Science. Copyright 2015 AAAS.

Today, the capabilities of electron microscopes (EMs) are being used to directly observe the structure of MGs. Recently, Hirata *et al.*[13] demonstrated that a single distorted icosahedron with partial FCC cubic symmetry could be directly observed for the $Zr_{80}Pt_{20}$ MG by using angstrom-beam electron diffraction in a double Cs-corrected EM, and this single distorted icosahedron was later proposed to be the frustration element contributing to glass-formation. Researchers have used 3D EM to observe the packing mechanism of advanced materials.[26–29] Now, combining and utilizing both 3D imaging and angstrom-beam diffraction, the fractal packing for MGs can be directly observed. These new observational abilities will help to unravel the mystery of atomic packing in MGs.

## 3. Structure stability of MGs

The study of MG structure stability can aid in exploring the development of new alloys with excellent GFA and the creation of the structure-property correlation for MGs. The studies of structure stability include two aspects: relaxation and crystallization. When heating an MG to the supercooled liquid region between glass transition $T_g$ and crystallization temperature $T_x$, the structure of glass first relaxes and then crys-

tallization takes place.[30–35] Novel microstructures and interfaces with an unusually large number of nanoscale precipitates could be synthesized using the principles of relaxation and crystallization studies. However, the atomic- to nano-scale mechanisms of relaxation and crystallization for MGs are long-standing issues for two reasons. First, whether or not the amorphous phase separation occurs during structural relaxation is unclear, because there is strong negative heating of mixing amongst the constituting elements.[36] Second, traditional nucleation theories cannot explain the crystallization behaviors for MGs that exhibit chemical and topological short-to-medium range order but lack long-range crystalline order.[37,38]

### 3.1. Amorphous phase separation

Amorphous phase separation in metallic glasses thus has been a controversial issue in the past several decades because of the large negative heat of mixing among its main constituent elements. Thermodynamics predicts that amorphous phase separation will never occur in an alloy system of the negative heat of mixing but also predicts that it is possible in an alloy system of the positive heat of mixing.[39,40] As shown in Tables 1 and 2, we reviewed papers about phase separation in metallic glasses. People support that the phase separation is possible for alloys with atomic pairs of the positive heat of mixing.[41–57] The strong positive heat of mixing among their constituent elements dramatically reduces the GFA, so the alloys in Table 1 are mainly ribbon size or limited bulk size. As listed in Table 2, the alloys of the strong negative heat of mixing could form bulk-size MGs.[36,58–66] Since 1969, Chen and Turnbull *et al.* proposed that there are unusual SROs in undercooled molten Pd–Si, Pd–Au–Si and Pd–Ni–P alloys,[58–60] which are responsible for the occurrence of amorphous phase separation before crystallization. Since the 1990s, Johnson *et al.*[65] also observed amorphous phase separation when annealing Zr-based multicomponent MGs in the supercooled liquid region. Thereafter, numerical evidence[66–69] was presented to support amorphous phase separation. Many of them were explored by microscopies.[67,69] However, the artifacts induced during sample preparation resulted in a lot of unclear results, thus stop supporting amorphous separation.[70]

To find trustworthy direct evidence is the key issue for resolving this long-standing issue. In 2003, Wang *et al.*[32] investigated the amorphous-to-crystalline transformation in BAM 11, i.e., $Zr_{52.5}Cu_{17.9}Ni_{14.6}Al_{10}Ti_5$, in the supercooled liquid region, using simultaneous x-ray diffraction and small angle scattering, which can reveal structure change from the atomic- to nano-scale simultaneously without inducing sample preparation issues for observation by microscopes. Figures 2(a) and 2(b) show that the intensity of small angle scattering profiles increases several minutes ahead of that of diffraction patterns. Later in 2009, Yang *et al.*[31] explained the origin of interference peaks in SAS profiles (Fig. 2(d)) using atom probe tomography (APT) (Figs. 2(e) and 2(f)). The core/shell particles with a depleted diffusion zone as shown in Fig. 2(e), instead of spinodal decomposition proposed by others before,[59] was observed during the transformation of nanocrystalline precipitates.

**Table 1.** MGs with atomic pairs of the positive heat of mixing.

| Composition | Sample size | Atomic pairs and heat of mixing/kJ·mol$^{-1}$ |
|---|---|---|
| $Zr_{60-x}Y_xAl_{15}Ni_{25}$, $15 \le x \le 35$[41] | ribbon and bulk ($\le$ 3 mm) | Z–Y (+9) |
| $Zr_{33}Y_{27}Al_{15}Ni_{25}$[42] | | |
| $La_{27.5}Zr_{27.5}Al_{25}Cu_{10}Ni_{10}$[43] | ribbon | Zr–La (+13) |
| $Y_{28}Ti_{28}Al_{24}Co_{20}$[44] | ribbon | Y–Ti (+15) |
| Ti–Y–Al–Co[45] | ribbon | Ti–Y (+15) |
| $Zr_{28}Y_{28}Al_{22}Co_{22}$[45] | | Zr–Y (+9) |
| Ni–Nb–Y[46] | ribbon | Nb–Y (+30) |
| Cu–Zr–Y–Al[47] | ribbon | Zr–Y (+35) |
| Cu–(Zr, Hf)–(Gd,Y)–Al[48] | ribbon | Zr–Y (+35) |
| | | Hf–Y (+11) |
| | | Zr–Gd (+9) |
| | | Hf–Gd (+11) |
| Nd–Zr–Al–Co[49] | ribbon | Nd–Zr (+10) |
| Zr–Y–Al–Co[50] | ribbon | Zr–Y (+35) |
| Zr–(Ce, Pr, Nd)–Al–Ni[51] | ribbon | Zr–RE (+) |
| Gd–Ti–Al–Co/Cu[52] | ribbon | Gd–Ti (+15) |
| Gd–Hf–Co–Al[53] | ribbon | Gd–Hf (+11) |
| Gd–(Hf, Ti, Y)–Co–Al[54] | | Gd–Ti (+15) |
| | | Gd–Y (0) |
| Zr–Gd–Al–Ni[55] | ribbon and bulk (1 mm) | Zr–Gd (+9) |
| Zr–Cu–Co–Al[56] | bulk (1 mm) | Co–Cu (+9) |
| Zr–Cu–Ni–Al–Fe[57] | bulk ($\le$ 2 mm) | Fe–Cu (+13) |

**Table 2.** Typical bulk MGs of the negative heat of mixing among its main constituent elements.

| Composition | Sample size | Atomic pair and mixing enthalpy/kJ·mol$^{-1}$ |
|---|---|---|
| Pd–Si[58] | ribbon or bulk | Pd–Si (–55) |
| Pd–Au–Si[59] | | Pd–Au(0) |
| | | Au–Si (–30) |
| Pd–Ni–P[36,60–63] | bulk (70 mm) | Pd–Ni (0) |
| | | Pd–P (–36.5) |
| | | Ni–P (–34.5) |
| Zr–Ti–Be[64] | bulk/cm | Zr–Ti (0) |
| Zr–Ti–Cu–Ni–Be[65] | | Zr–Cu (–23) |
| | | Zr–Ni (–49) |
| | | Zr–Be (–43) |
| | | Ti–Cu (–9) |
| | | Ti–Ni (–35) |
| | | Ti–Be (–30) |
| | | Cu–Ni (+4) |
| | | Cu–Be (0) |
| | | Ni–Be (–4) |
| Zr–Ti–Cu–Ti–Al[31,32,66] | bulk/cm | Zr–Ti (0) |
| | | Zr–Cu (–23) |
| | | Zr–Ni (–49) |
| | | Zr–Al (–44) |
| | | Ti–Cu (–9) |
| | | Ti–Ni (–35) |
| | | Ti–Al (–30) |
| | | Cu–Ni (+4) |
| | | Cu–Al (–1) |
| | | Ni–Al (–22) |

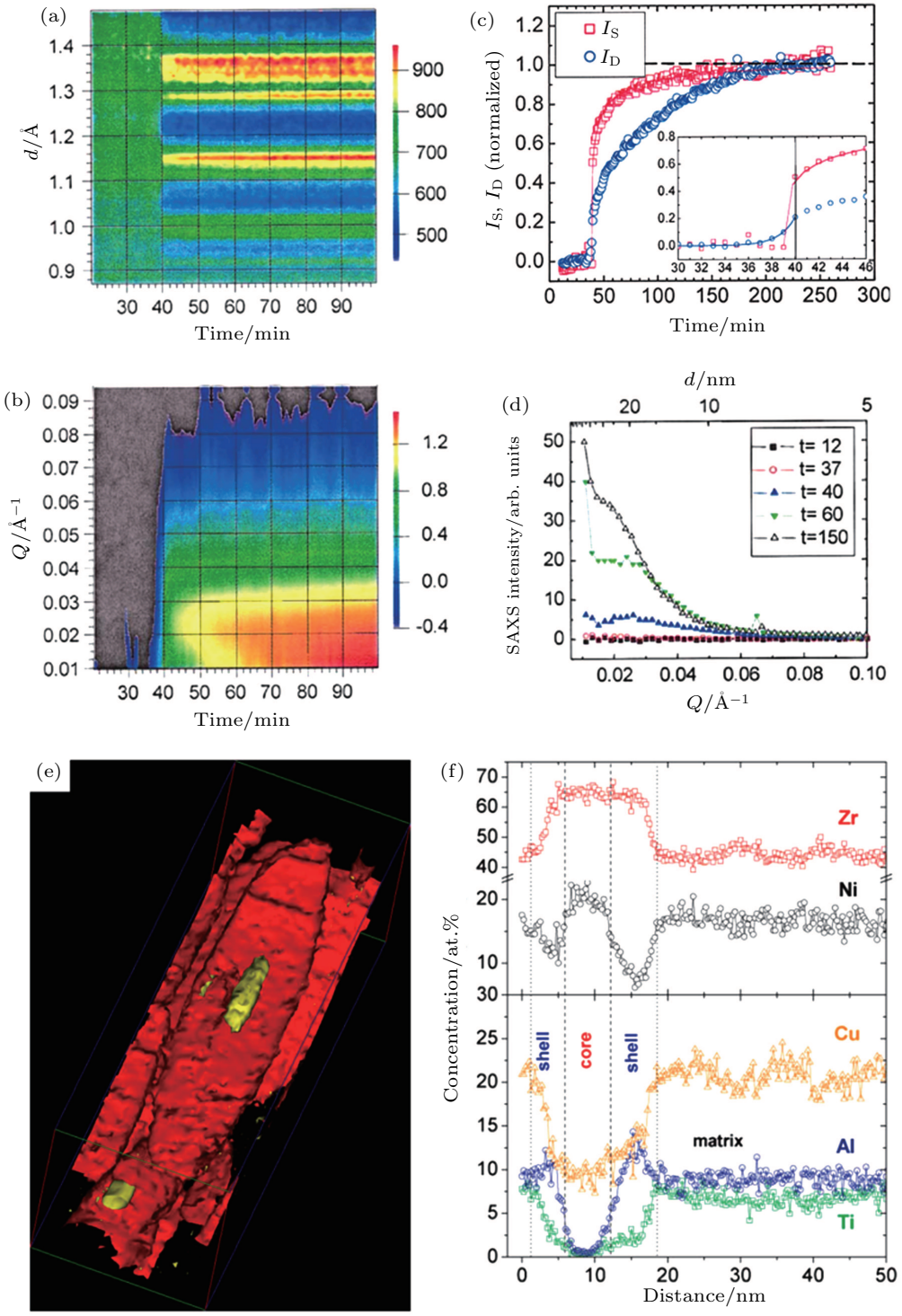



**Fig. 2.** (color online) Simultaneous diffraction and SAXS data for BAM 11 during annealing.[31,32] With permission from Physical Review Letters. Copyright 2003 American Physics Society. Also with permission from Advanced Materials. Copyright 2009 Wiley Online Library. (a) 2D map of diffraction pattern as a function of annealing time. (b) 2D map of SAXS profiles as a function of annealing time. (c) Normalized integrated of the intensity of diffraction and SAXS as a function of time based on Figs. 2(a) and 2(b). It shows intensity increasing the time difference of diffraction and SAXS. (e) 3D AP composition mapping of a nanocrystalline particle in the annealed BAM 11 MG. (f) Composition mapping results for constituent elements of a nanoparticle in BAM 11.

The existence of amorphous phase separation is a long-standing issue for Pd–Ni–P alloys. In 1976, Chen *et al*. proposed the possibility of amorphous phase separation in Pd-based alloys.[60] Later, researchers countered this possibility, finding that efforts were made in the samples using cooling paths as shown by path (i) and (ii) in Fig. 3(a).[71–73] Amorphous phase separation cannot be observed in MGs using these transitional paths for cooling and subsequence annealing. In 2012, Lan *et al*.[36] found out that there is possible amorphous phase separation in Pd–Ni–P MGs using cooling paths as shown by the path (iii) in Fig. 3(a), in which the high-temperature liquid was quenched to the supercooled liquid

region directly to perform subsequence annealing in the intermediate target temperature. When the annealing temperature is in the proposed miscibility gap,[74] then amorphous phase separation occurs. As shown in Figs. 3(b) and 3(c), by high angle annular dark field image using scanning transmission microscopy mode, brightness and darkness fluctuations can be observed, and there is composition variation in the MGs with long enough annealing time $\sim 200$ s.[75] Recently, Wu *et al.*[76] confirmed this observation by using SAXS and proposed a spinodal decomposition mechanism for the amorphous decomposition in Pd–Ni–P MGs. The interference peak identified at $\sim 0.085$ nm$^{-1}$ is consistent with the correlation length observation results by Lan *et al.*[36] and Lau *et al.*[74] Although evidence has been observed in a Pd–Ni–P MG with strong negative heat of mixing prepared using cooling path (see path (iii) in Fig. 3(a)), the origin of the occurrence of amorphous phase separation is still a mystery. The evidence of amorphous phase separation in MGs prepared using path (i) and (ii) is still lacking, so we still need to determine the origin of the asymmetry of heating/cooling in these Pd–Ni–P alloys.

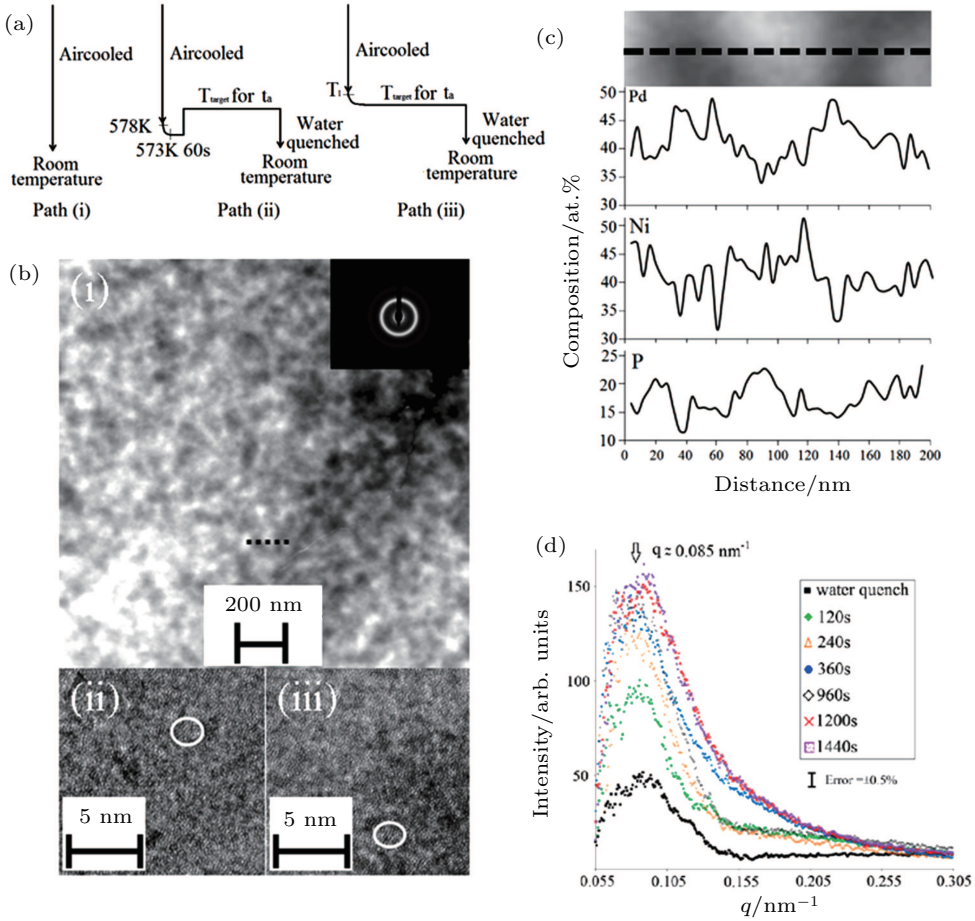



**Fig. 3.** (color online) Amorphous phase separation occurred in $Pd_{41.25}Ni_{41.25}P_{17.5}$ metallic glasses.[36,76] (a) Three typical cooling and annealing paths. (i) Quenching from liquid to solid; (ii) quenching to a temperature below $T_g$ and heating it back to the supercooled liquid region for annealing; (iii) cooling high temperature liquid to the supercooled liquid region and annealing it at the intermediate target temperature in supercooled liquid region. (b) STEM-HADDF image (i) and HRTEM images (ii and iii) of a $Pd_{41.25}Ni_{41.25}P_{17.5}$ MG using cooling and annealing path (iii) in Figs. 3(a) and 3(c). EDX mapping results for elements in the $Pd_{41.25}Ni_{41.25}P_{17.5}$ MG. The mapping path is listed in (i) of Fig. 3(b), with permission from Journal of Non-Crystalline Solids. Copyright 2012 Elsevier. (d) SAXS profiles for $Pd_{41.25}Ni_{41.25}P_{17.5}$ MG using cooling path (iii) in Fig. 3(a) at different annealing times. An interference peak was determined at $\sim 0.085$ nm$^{-1}$. With permission from Journal of Non-Crystalline Solids. Copyright 2014 Elsevier.

### 3.2. Multi-stage crystallization process

Another interesting aspect is how the decomposition in an amorphous state affects subsequent crystallization. The occurrence of nano-scale amorphous phase separation may enhance the rearrangement of chemical species prior to crystallization in BAM-11 and help the system to achieve a new metastable equilibrium. Initially, the chemical composition of the alloy is homogeneous due to the fast quenching rate. During annealing, like-clusters (solute-centered SRO) are prone to stay together and to connect to be a network, perhaps by following these possible proposed mechanisms: a single atom jump[77] of neighboring mobile atoms between clusters, e.g., solvents, the fast diffusion of small interstitial atoms,[78] and the creation/annihilation of "defects" like free volume.[79–81] These mobile atoms play the role of "connecting atoms." "Connecting atoms"[82] are easier to be obtained for patching the "imperfect" or "weaker" region (e.g., "holes" and "cavities"). Having begun patching a region, then larger scale clusters

(∼nm scale) can be formed, thus further enhancing the connectivity of the network.[83] Finally, different networks characterized by different building blocks, i.e., solute-centered SROs, would intertwine with each other at the nanometer scale and then fill in the whole space. One of the networks is mainly formed by Cu and Ni centered clusters, and another network is rich in Al and Ti centered clusters. Based on the framework of amorphous phase separation, we propose two stages for phase transformations at the early stage of crystallization of bulk MGs, such as BAM-11, as follows:

i) the formation of a metastable phase;

ii) a stabilized crystalline phase with complex structure.

At the first stage, a metastable phase would be incubated, which was proposed as a large cube structure[84] packed by solute-centered clusters such as icosahedral SRO. As pointed by Sheng *et al.*,[20] the 'full' icosahedra with complete five-fold symmetry formed to frustrate crystallization ordering due to the size effect of constituent elements. In the beginning, there should be a lot of full icosahedra for the multi-component alloy with a variation of atomic size. The final state of BAM 11 was identified as t-$Zr_2Ni$ phase.[31] There are large discrepancies between the initial state and the final state of alloy either in chemical and topological. The amorphous phase separation may pave the way for the transformation of metastable phases by reducing the chemical disordering. To some degree, most of the full icosahedra would be destroyed to be distorted forms because of the reducing size effect by phase separation during annealing. It is possible to reconstruct the distorted icosahedra with incomplete five-fold symmetry to transform it into a more stable phase with higher crystalline ordering.[85,86] So the formation of metastable phase such as a big cube phase with distorted icosahedra may lower the nucleation barrier and further favor the crystallization process.

Nanoscale solute partition happens at the second stage due to the difference of the heat of mixing (as shown in Table 2) between constituent elements. For BAM 11, the chemical composition of the core of precipitates was proposed to be similar to $Zr_2M$. M represents solute atoms rich in Ni, Cu, but poor in Al, Ti. The solute partition process after crystallization in BAM 11.[31,32] can be observed using small angle scattering (Fig. 2(d)) and composition mapping of APT (Fig. 2(f)). To achieve long-range ordering, more and more appropriate atoms (Zr, Ni, etc.) will be added into the crystalline clusters. At the same time, more and more specific solute atoms (Ti, etc.) will be rejected outside the crystalline clusters. So a diffusion zone will be formed between the matrix and the crystalline cluster. Finally, the core of the crystallite has a much higher ordering than the shell, and the matrix remains in a higher disordering state for multi-component alloys such as BAM 11. The formation of core/shell structure proves that the diffusion in an MG with excellent GFA is extremely hard, thus hindering the growth of precipitates. This crystallization mechanism results in huge number density ($10^{23}$–$10^{24}$ $m^{-3}$) of nanocrystalline precipitates, evenly distributed in glassy matrix.[87,88]

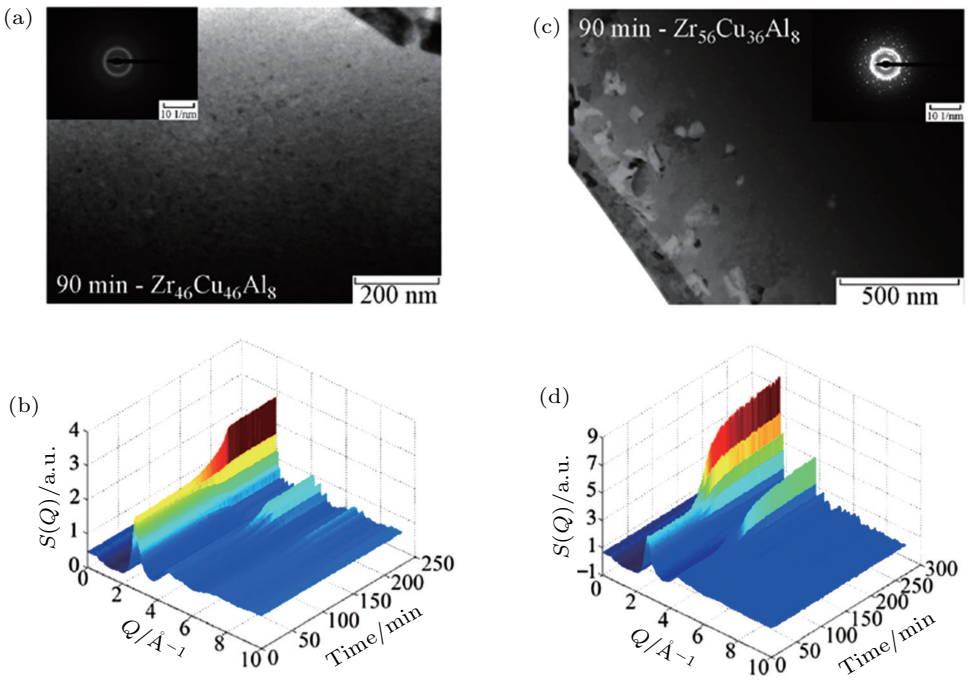



**Fig. 4.** (color online) Crystallization pathways in Zr–Cu–Al BMGs.[90] (a) Bright-field TEM image and (c) 3D map of diffraction patterns using times-resolved neutron scattering together, revealing a classic crystallization pathway in a marginal glass former, $Zr_{56}Cu_{36}Al_8$ alloy. (b) Bright-field TEM image and (d) 3D map of diffraction patterns using time-resolved neutron scattering together revealing an unusual (i.e., avalanche nucleation) crystallization pathway in a good glass former, $Zr_{46}Cu_{46}Al_8$ alloy. With permission from Applied Physics Letters. Copyright 2014 AIP Publishing.

Because the structure of supercooled liquid is completely different from that of crystals, it is difficult to form a complex crystalline phase directly, especially for those MGs that have good GFA. Recently, the MD simulation by Tang *et al.*[89] of interfacial structure for two alloys, Ni–Al and Zr–Cu, with difference GFA showed that the crystalline ordering in the Zr–Cu with better GFA just extended to limited atomic layers. For Zr–Cu alloy, there is no pre-crystalline ordering in its liquid compared to that of the Ni–Al alloy. It is reasonable that a metastable phase may be formed for Zr–Cu prior to the final crystalline phase to lower crystal/liquid interfacial energy. Recently, Lan *et al.*[90] observed a 'suspicious' metastable phase for Zr–Cu–Al MG. As shown in Fig. 4(a), a large number of 'black dots' were observed by *in situ* TEM for a good glass former $Zr_{46}Cu_{46}Al_8$ alloy. The inset of Fig. 4(a), showing a select area electron diffraction pattern (SAED), illustrates that there is no obvious crystalline ordering for the nanoscale precipitates. Figure 4(b) shows TEM image and SAED of precipitates for the average glass former $Zr_{56}Cu_{36}Al_8$ with larger grain size and much higher ordering. The crystallization for $Zr_{56}Cu_{36}Al_8$ was identified to be a continuous nucleation and growth pathway using time-resolved neutron scattering as shown in Fig. 4(c). However, the final crystalline phase $Zr_{46}Cu_{46}Al_8$ has a more complex structure and thus results in an unusual crystallization pathway as shown in Fig. 4(c), which is a site-saturated nucleation process. The growth for the 'black dots' $Zr_{46}Cu_{46}Al_8$ is 'avalanche-like' and finally, they are pinned to each other as illustrated by the plateau of peak intensity in Fig. 4(c). The hints of 'avalanche-like' crystallization have been observed before for colloid systems[91] and also MGs such as BAM 11.[32] As shown in Figs. 4(a) and 4(c), the appearance of the Bragg peak is sudden, and the normalized intensity of the Bragg peak tends to be a plateau. The avalanched nucleation is studied in Wang's group.[38] for a series of Zr–Cu–Al alloys with a change of GFA using time-resolved neutron scattering and *in situ* TEM. We thus propose that the unusual crystallization characterized with avalanche nucleation and complex crystalline structure would be correlated to MGs with excellent GFA. The formation of a metastable phase during crystallization would be the origin of the avalanche nucleation behavior.

## 4. Liquid–liquid phase transition

LLPT is defined as the transition between two liquid states with different density and entropy. LLPT has been proposed, in principle, to be a general phenomenon in all kinds of liquid.[92,93] The existence of LLPT was reported in a variety of liquids from atomic to molecular liquids, including P,[94] C,[95] Si,[96,97] Ge,[98,99] $SiO_2$,[100] $GeO_2$,[101] $H_2O$,[93,102–104] $Al_2O_3$-$Y_2O_3$,[105] triphenyl phosphite (TPP),[106,107] etc. LLPT is usually accompanied by the poly-amorphous transition, i.e., liquid polymorphism. Experiments and simulations together showed that there are structure changes[94–96,98,100–102,104–106,108–110] during the occurrence of LLPT, sometimes accompanied by the changes of physical properties such as density and specific heat. Katayama *et al.*[94] directly observed the coexistence of two forms of liquids, i.e., molecular and polymeric phosphorus liquids, with totally different structures using *in situ* x-ray diffraction. Although numerical supporting evidence was reported, there were still many reports contradicting such evidence, especially in Si,[111] $H_2O$,[104,112] $Al_2O_3$-$Y_2O_3$,[113] TPP,[114] etc. LLPT and the liquid polymorphism are still controversial issues because consistently direct observations are few and the nature of the occurrence of LLPT is unclear.

Many theories, including frustration,[18,19] a two-order-parameter model[115–119] and a random first-order transition (RFOT),[120] etc., have been suggested to explain the structure and dynamic evolution of liquid when LLPT occurs. According to frustration theory,[18,19] there exist dynamic, locally preferred structure (LPS), such as icosahedra, which differ from that of crystalline phases. LPS cannot perfectly tile to the whole space and thus give rise to an abstract reference system in which the effect of frustration has been turned off. Therefore, there exists an avoided critical point for the occurrence of a weakly first-order phase transition in a liquid state. One of the structural origins of LLPT proposed by a two-order parameters theory via Tanaka *et al.*[92] is the cooperative development of short- to medium-range ordering (SRO and MRO) and the frustration/competition of these so-called locally/energetically favored structures with density ordering. The two-order-parameter model has been used successfully to describe water's anomalies.[121] The lack of theory connecting structure and dynamic makes the explanation of the LLPT difficult. RFOT[120] was developed for predicting relationships connecting the $\alpha$ relaxation time $\tau_\alpha$, the static length scale $\xi_s$ and the configuration entropy $S_c$ (as introduced by Adam-Gibbs relation[122]) RFOT introduced an interface free energy cost between two amorphous/liquid phases, which is hard to describe with a usual order parameter. RFOT thus provides a different possible way to unravel the structure origin of LLPT.

The poly-amorphous phase transition in MGs was first reported by Sheng *et al.*[123] in a $Ce_{55}Al_{45}$ alloy induced by high pressure using *in situ* x-ray diffraction. Abrupt shifts of the first sharp diffraction peak position $Q_1$ as well as a crossover in calculated specific volume have been observed as a function of hydrostatic pressure. The structure and density changes together indicated the occurrence of polyamorphous phase transition. The possible origin revealed by *ab initial* MD simulation is f-electron delocalization of Ce. Later, the "polyamorphism" in a $Ce_{75}Al_{25}$ MG has also been observed by Zeng *et al.*[124] The direct experimental evidence of 4f-electronic delocalization was elaborated. If the f-electron delocalization

gives rise to the compressibility for MGs under pressure, is the LLPT or polyamorphous transition possible in MGs without f-electron delocalization property? What is the possible origin for an LLPT induced by temperature instead of induced by pressure?

F–S transition has been reported in numerical references based on viscosity studies,[108,110,125–130] which implies the occurrence of a dynamic transition in MGs. Until recently, Li *et al.*[131] demonstrated that LLPT is possible in MGs during heating/cooling based on volumetric measurements results using electro-levitation for three Zr-based alloys ($Zr_{42.6}Ti_{12.4}Cu_{11.2}Ni_{10}Be_{23.8}$ (Vit 1), $Zr_{57}Nb_5Al_{10}Cu_{15.4}Ni_{12.6}$,(Vit 106), and $Zr_{49.1}Ti_{7.67}Cu_{16.3}Ni_{13.2}Al_7Be_{6.8}$ (LM 7)). Later, structure evidence of an LLPT was also observed in a variety of metallic glass forming liquids (MGFLs) during heating/cooling, including, Vit 1,[132] $Zr_{50}Cu_{40}Al_{10}$,[133] $La_{50}Ni_{35}Al_{15}$,[134] Vit 106,[135] etc.

Wei *et al.*[132] reported an LLPT in the Vit 1 MGFL, and correlated the structure changes with a specific heat $C_p$ maxima about $T_m$. The abrupt change of $Q_1$ in $S(Q)$ observed during cooling was around 800 K and shifts to larger $Q$ values, indicating that the structure change corresponds to a transition from the high-density liquid (HDL) to low-density liquid (LDL). The full width at half maximum (FWHM) also showed that increase with decreasing, which means that the low-temperature more ordered liquids have shorter correlation length, which is related to the characteristic size of SRO and MRO. Unfortunately, these observations are difficult to reconcile with current views of LLPT.

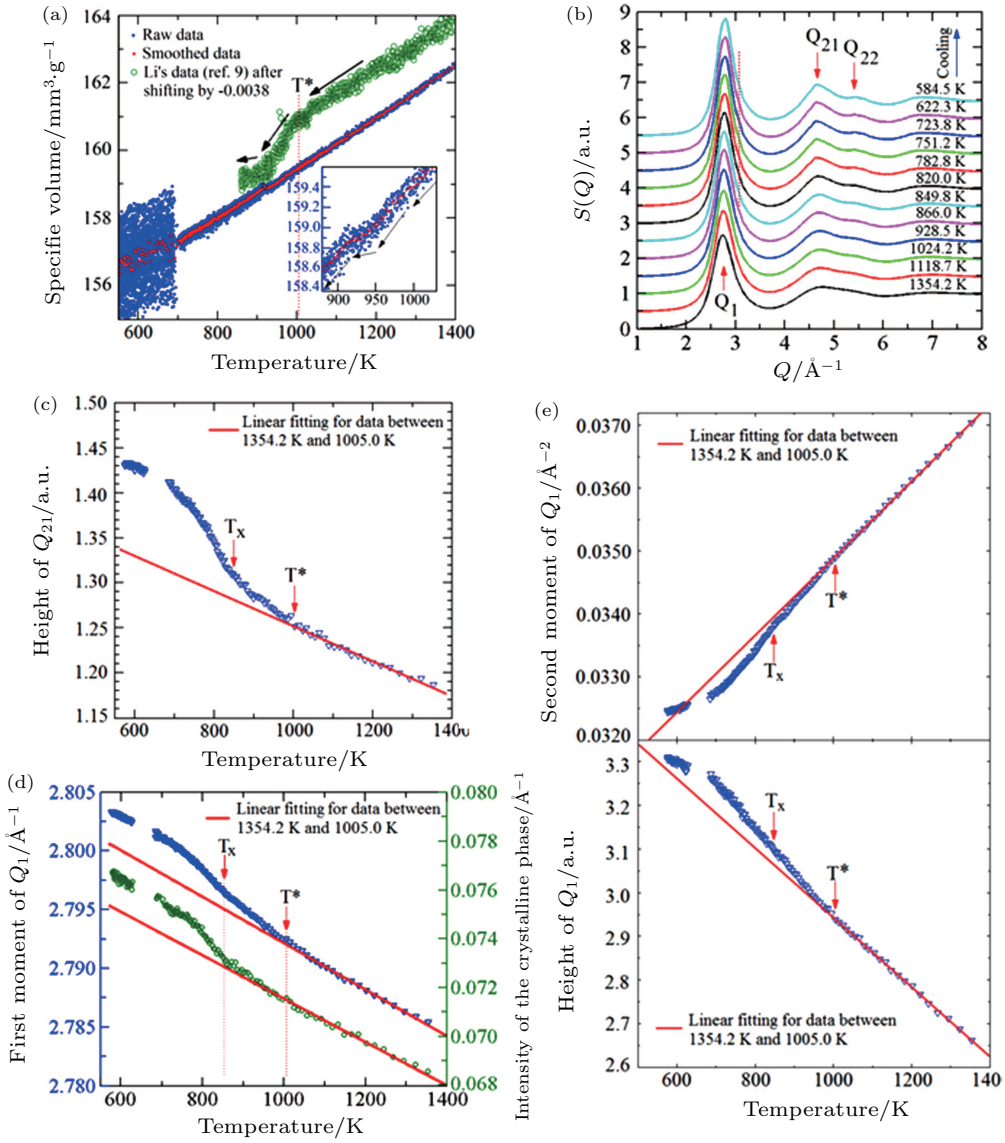



**Fig. 5.** (color online) Structure evolution and specific volume measurements during cooling.[135] (a) The specific volume as a function of temperature for VIT 106 liquid under cooling. A kink at $\sim$ 1000 K has been indicated by the red dotted line. (b) Total scattering patterns under cooling. Red arrows indicate the name of the peaks. Blue arrow shows the development direction of diffraction patterns during cooling. (c) The relation between the height of $Q_{21}$ and temperature during cooling. Red arrows indicate the position of the occurrence of structure changes. The red line is the linear fitting. (d) The first moment of $Q_1$ as a function of temperature. The first moment was calculated using equation: $Q_1 = \Sigma S(Q) \cdot Q / \Sigma S(Q)$ (e) The second moment and height of $Q_1$ as a function of temperature. The second moment was calculated using equation: $\sigma^2 = \Sigma S(Q) \cdot (Q - Q_1)^2 / \Sigma S(Q)$. Red arrows indicate the position of the occurrence of structure changes. The red line is the linear fitting. With permission from Applied Physics Letters. Copyright 2016 AIP Publishing.

Wu *et al.*[134] identified evidence of an LLPT accompanied by larger changes in atomic diffusion behavior using high-temperature NMR in the $La_{50}Ni_{35}Al_{15}$ MGFL above its $T_m$. A two-order parameter model[92] was used to explain the occurrence of the LLPT based on the revealed bond orientation order changes at transition temperature by *ab initial* MD simulations. The crystallization due to supercooling could be ruled out because of the occurrence of LLPT above $T_m$.

We studied the structure evolution and specific volume changes for Vit 106 MGFL using electrostatic levitator.[135] Combining with the MD simulation for the $Zr_{57}Cu_{28}Al_{15}$ alloy, approximating the Vit 106 alloys as a pseudo-ternary alloy $Zr_{57}(Cu_{15.4}Ni_{12.6})(Nb_5Al_{10})$ by consideration of the atomic radius of constituents,[16] consistent concrete evidence has been identified for the occurrence of LLPT in the supercooled liquid. As shown in Fig. 5(a), specific volume measurements are consistent with Li *et al.*'s observation. A kink was identified to be $\sim$ 1000 K, which is denoted as $T^*$. To avoid the inducing of analysis error by applying any functions to fit the peak position and peak width for the diffraction maxima in $S(Q)$, the first and second moments have been used for representing the evolution of peak position and peak width. The height of peak 2 in $S(Q)$ (Fig. 5(c)) shows an abrupt change $\sim T^*$, which is consistent with $T^*$ identified by the evolution of the first moment (Fig. 5(d)) and second moment (Fig. 5(e)) as well as the height of peak 1 (Fig. 5(e)) in $S(Q)$. The peak position changes suggest a transition of LDL to HDL in Vit 106 liquid during cooling. The peak width changes indicated that the correlation length of the development of HDL increases and deviates from the usual linear relationship at $\sim T^*$. Moreover, a careful analysis was applied to check the occurrence of nano-crystallization during cooling, which was little discussed in the other studies.[132,133] It was found that there is a crystallization temperature $\sim$ 850 K. By subtraction of the high-temperature diffraction pattern, the subtle Bragg peak can be determined as shown in Fig. 6(a), and figure 6(b) suggests a few crystalline phases. The evolution of Bragg peak as a function of temperature is superimposed to Fig. 5(d) for comparison.

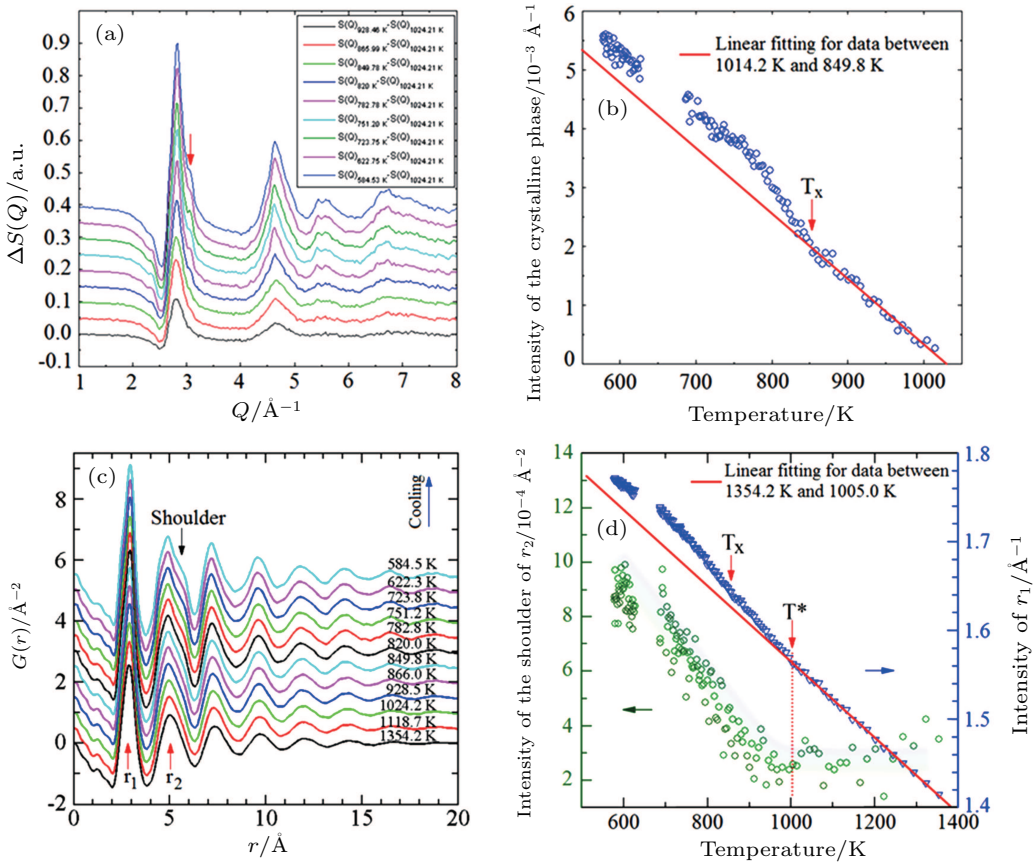



**Fig. 6.** (color online) (a) The $\Delta S(Q)$ curves at different temperatures, calculated by subtracting the $S(Q)$ at 1024.21 K, which is above $T^*$. The red arrow indicates the position of a Bragg peak developed below $\sim$ 850 K. This method is sensitive to as low as $10^{-6}$ volume fraction transformed. (b) The integrated intensity of the identified crystalline peak in $\Delta S(Q)$. The $T_x$ indicated by a red arrow shows the onset temperature of crystallization. The red line is a linear fit of data above $T_x$. (c) The evolution of liquid ordering can be observed using reduced PDFs ($G(r)$). The red arrows indicate the first ($r_1$) and second ($r_2$) coordination shells. The black arrow identifies a shoulder peak that formed below $T^*$. (d) The integrated intensities of the shoulder peak of $r_2$ (green circles) and the first peak $r_1$ (blue triangles) as a function of temperature during cooling. With permission from Applied Physics Letters. Copyright 2016 AIP Publishing.

The nature of LLPT has also been proposed to be the enhancement of connectivity of solute-centered clusters in medium-range scale. As shown in Fig. 6(c), the evolution of liquid ordering can be observed using reduced PDFs $(G(r))$ which were obtained by Fourier transformation $Q(S(Q)-1)$.

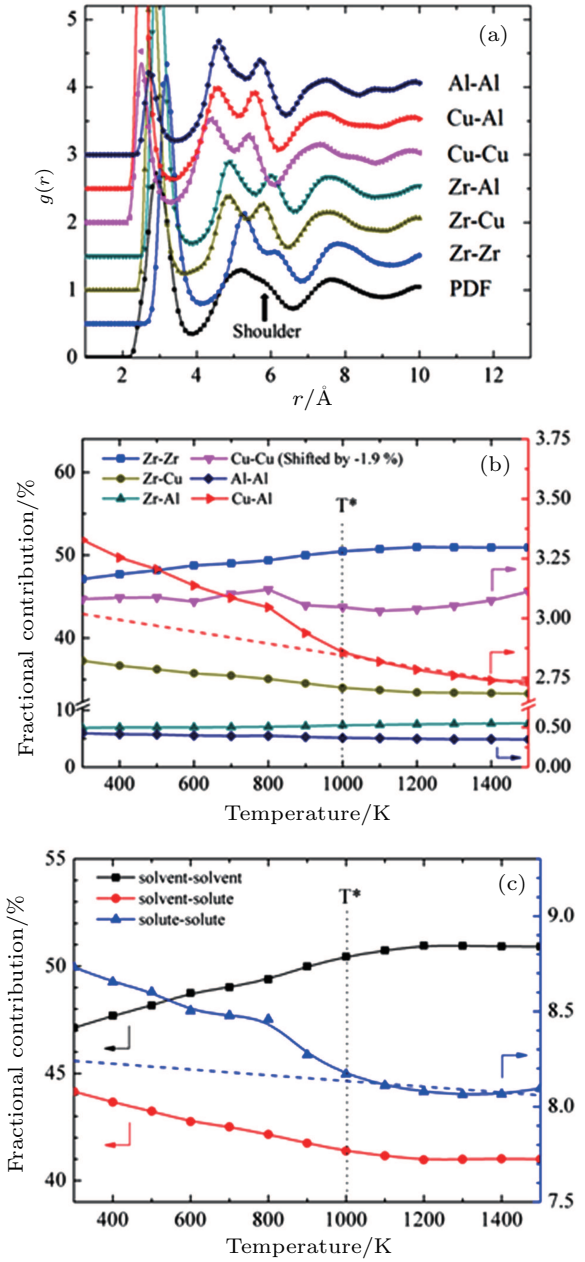



**Fig. 7.** (color online) (a) PDF, $g(r)$, and partial PDF of EAM MD-derived configurations are plotted. The position of the PDF shoulder has been indicated by the black arrow. (b) Development of the fractional contribution (adding up to 100%) of partial PDFs at the shoulder position. The partial PDFs were weighted by the x-ray scattering factors and compositions for each atomic pairs. The transition temperature, $T^*$, from the experimental data, is marked. As temperature decreases, the fraction of solute-solute atomic pairs, notably Cu–Al, increases. The dotted line is a linear fit of Cu–Al data for $T > 1000$ K, to highlight the increase of Cu–Al pair at $T^*$. (c) Fractional contributions (adding up to 100%) of partial pair distribution functions at the shoulder position $r = 5.70$ Å obtained from MD simulations. Different types of atomic pairs: solvent–solvent (Zr–Zr), solvent-solute (Zr–Cu and Zr–Al), and solute-solute (including Cu–Al, Cu–Cu, and Al–Al). The transition temperature, $T^*$, from the experimental data, is also marked by the vertical dotted line. The dashed line is a linear fit of the solute-solute pairs at temperatures above $T^*$. With permission from Applied Physics Letters. Copyright 2016 AIP Publishing.

The integrations of intensity for coordination shells illustrate that there is an abrupt increase of intensity for the shoulder of the second neighbor shell as shown in Fig. 6(d), suggesting the sudden enhancing of SRO connectivity. The continuous growing of SRO has been reported by using MD simulations for ZrCu MGs.[136]. However, there is rare report related to the phenomenon as observed in our study. MD simulations performed in $Zr_{57}Cu_{28}Al_{15}$ melt identified the partial PDFs $(g(r))$ during cooling. By examining the atomic weight factors of different elements, the contributions of different atomic pairs for the shoulder peak in PDFs $\sim 5.7$ Å$^{-1}$ were calculated as shown in Fig. 7(b). The solute in $Zr_{57}Cu_{28}Al_{15}$ melt is Cu and Al. The proportional contributions from solute-solute, solvent-solute, and solvent-solvent atomic pairs can be easily obtained by summing up the contributions from different atomic pairs. We can clearly distinguish the evolution behavior of different types of atomic pairs at $\sim T^*$. The solvent-solvent atomic pair tends to decrease at $\sim T^*$ while the contributions of the solvent-solute atomic pair and solute-solute atomic pair show an accelerating increasing when LLPT occurs.

## 5. Mechanical properties of metallic glasses

There are excellent reviews on the mechanical properties of MGs in recent years. A comprehensive discussion of elastic property is provided in Ref. [137]. References [138] and [139] emphasized the deformation and fracture mechanisms. The authors also constructed a deformation map.[138] Reference [140] summarized the progress in understanding shear bands. In this part, we will offer a brief summary of the overall mechanical behavior of MGs. For more detailed information, the readers can go to the review articles shown above.

### 5.1. Elastic deformation

One of the most impressive mechanical properties of MGs is their high yield strength. Figure 8(a) shows the Ashby map of elastic limit versus Young's modulus of different alloys.[141] MGs always show a higher elastic limit, which approaches the theoretical strength, than their crystalline counterparts. The high elastic limit comes from the amorphous structure of MGs. There are no grain boundaries or dislocations, which commonly carry plastic deformation, in MGs. Recent studies further found that the elastic deformation is inhomogeneous in MGs. By x-ray diffraction and anisotropic pair-density function analysis, Dmowski *et al.* showed that about a quarter in volume fraction of metallic glasses deforms anelastically.[142,143]

The bulk modulus of MGs is usually several percents smaller than the corresponding crystalline alloys.[144] This can be understood by the fact that MGs usually have a lower density, about 0.5%–2%, than their crystalline counterparts.[145] In other words, the average interatomic distance in amorphous

structure is slightly larger than in the crystalline structure, resulting in a slighter change of atomic potential when atoms are moving towards or apart from each other under external hydrostatic stress. The shear modulus of MGs is, however, about 30% smaller than the corresponding crystalline alloys.[138] The significant decreasing of shear modulus in MGs indicates a different mechanism of atomic movement under shear stress. Ma *et al.*[146] showed that a variety of BMGs inherit their Young's modulus and shear modulus from the solvent components. They attributed this to preferential straining of locally solvent-rich configurations among tightly bonded atomic clusters by x-ray diffraction. The x-ray diffraction results of MGs during elastic deformation are presented in Fig. 8(b). It is found that the first peak of the longitudinal structure factor changes with stresses, while the high-$q$ part remains almost unchanged. As discussed above, the first diffraction peak in $S(q)$ describes the medium-range atomic arrangement, while the high-$q$ part reflects the SRO. The results indicate the MRO is elastically deformed by a uniform strain, while, on the other hand, that atomic clusters (SRO) behave in a much stiffer manner. The schematic picture of atomic clusters arrangement of amorphous structure is shown in Fig. 8(c), which indicates the bonds between solvent atoms in solute-centered clusters B and super-clusters C constitute the weakest link in an amorphous structure.

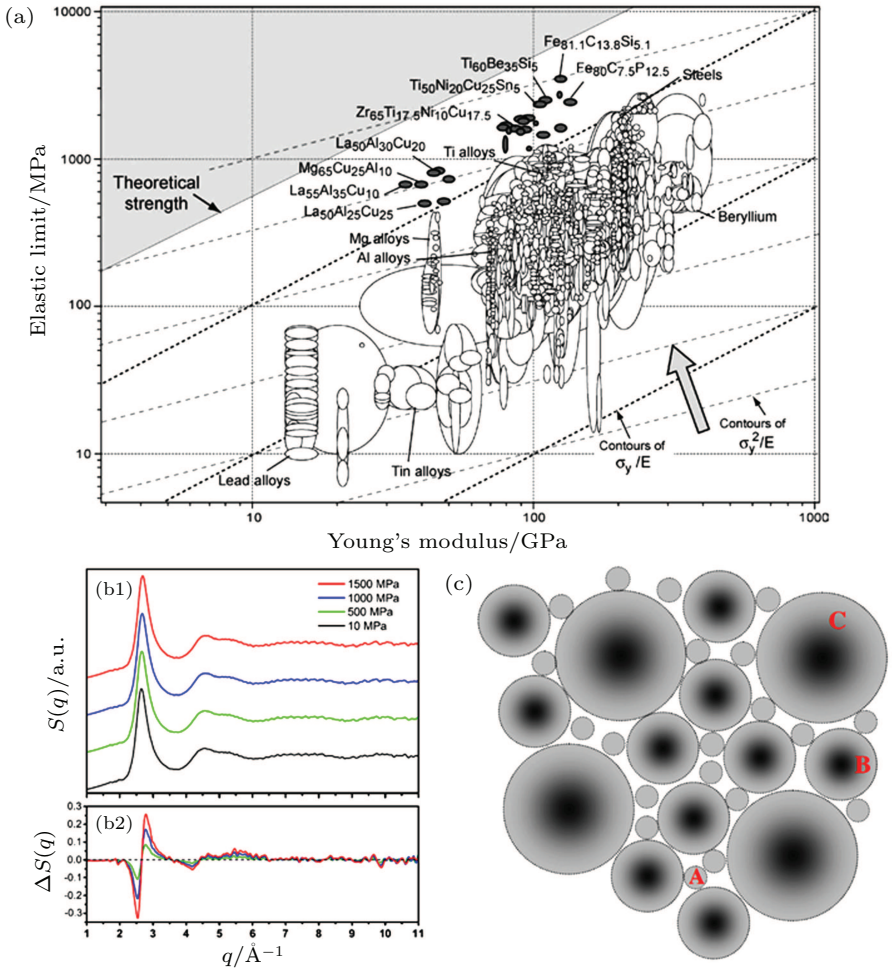



**Fig. 8.** (color online) (a) Ashby map of elastic limit versus Young's modules of different alloys.[141] With permission from Scripta Materialia. Copyright 2006 Elsevier. (b1) The longitudinal structure factor $S(q)$ under a compressive stress of 10, 500, 1000, and 1500 MPa, respectively. (b2) Difference plot of $S(q)$, between 10 MPa and higher stress levels. (c) Schematic illustration of a hypothetical amorphous structure showing local packing of solvent atoms ($A$), solute-centered clusters ($B$), and super-clusters ($C$) in a metallic glass. The gray color in B and C denotes the outmost atomic shell filled with a majority of solvent atoms. The dark spot in B represents the solute atom of a solute-centered cluster, while the dark area in C represents the inner solute-enriched region within a super-cluster.[146] With permission from Physical Review Letters. Copyright 2012 American Physics Society.

### 5.2. Plastic deformation

Depending on sample condition, temperature and strain rate, the plastic deformation of metallic glasses can be roughly divided into inhomogeneous flow and homogeneous flow.

Inhomogeneous flow usually occurs when the temperature is far below glass transition temperature and the strain rate is relatively fast. The basic unit of plastic deformation is believed to be a single atom hopping according to the free volume model[147,148] or a group of atoms shearing collectively according to the shear transformation zone (STZ) model,[149] driven by external stresses. In both models, shearing will induce dilatation which is characterized by increasing free

volume. When the increasing of free volume is faster than annihilation, the free volume in local regions will accumulate and result in a lower viscosity. These locally softened regions then flow more easily compared to the surrounding matrix. Upon yielding, a thin sheared region called shear band is then formed from the locally softened regions with a higher content of free volume to carry the plastic strain. This is unlike the plastic deformation in crystalline alloys, in which plastic strain is compensated by dislocation sliding, grain boundary motion, Martensite–Austenite transformation, etc. Because the shear band is soft and localized, MGs are usually brittle at room temperature. However, there are some systems showing large plasticity under uni-axial compression and high fracture toughness.[150,151] Figure 9(a) is a stress-strain curve of Pt–Cu–Ni–P BMG.[152] It shows a large plastic strain up to 20%. BMGs with large compressive plasticity were also reported in Pd-based,[153–155] Zr-based,[156–164] Ni-based,[165–168] Cu-based,[169,170], Fe-based,[171,172] Co-based,[173] Mg-based,[174] Ti-based,[175–180] and Hf-based[181] alloy systems.

It was found that BMGs with a large poisson ratio will exhibit large compression plasticity.[182] The plasticity was also found to be influenced by fabrication processes. A higher cooling rate may result in a greater plasticity.[154] Phase separation is another factor which was proposed to enhance the plasticity because of the existence of the finely distributed amorphous network structure. However, recent study on phase separated Pd-based BMGs shows that the amorphous network with two brittle MGs cannot stop the propagation of shear bands. As indicated in Fig. 9(b1), the HAADF image of a phase separated Pd–Ni–P BMG shows a network like structure with a wavelength about 100 nm. Figure 9(b2) is the corresponding stress-strain curve under compression, showing it is brittle.[183]

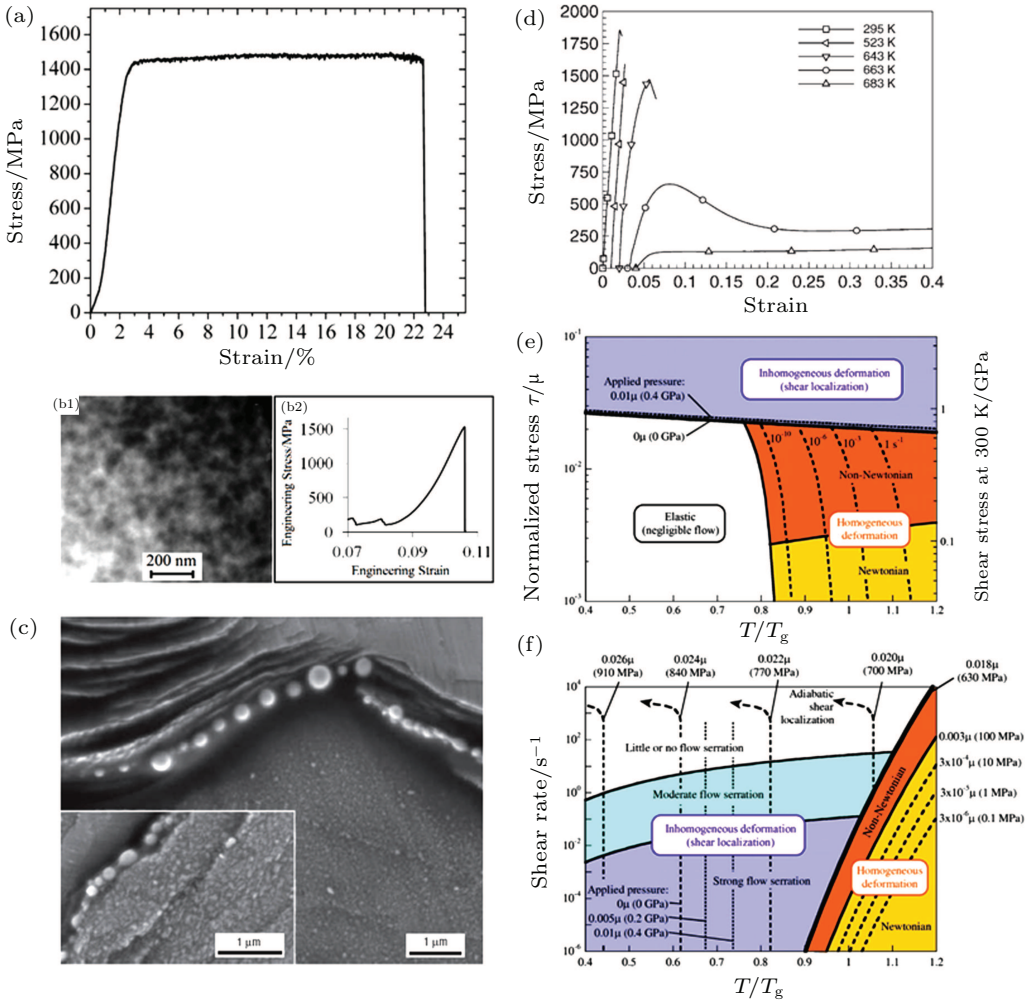



**Fig. 9.** (color online) (a) Stress-strain curve of amorphous monolithic $Pt_{57.5}Cu_{14.7}Ni_{5.3}P_{22.5}$.[152] With permission from Physical Review Letters. Copyright 2004 American Physics Society. (b1) HAADF image of $Pd_{41.25}Ni_{41.25}P_{17.5}$ phase separated BMG; (b2) stress-strain curve of $Pd_{41.25}Ni_{41.25}P_{17.5}$ phase separated BMG.[183] (c) Scanning electron micrographs showing details of shear bands after local melting of the tin coating. The inset shows the shear-band pattern and tin beads located in regions removed from the large shear offset shown at the top of figure.[185] With permission from Nature Materials. Copyright 2006 Nature Publishing Group. (d) Effect of temperature on the uniaxial stress-strain behavior of Vitreloy 1 at a strain rate of $1.0 \times 10^{-1}$ $s^{-1}$ and temperatures $T = 295$, 523, 643, 663, and 683 K. The stress–strain curves have been shifted to the right to avoid overlapping curves of similar shapes and sizes.[191] With permission from Acta Materialia. Copyright 2003 Elsevier. Deformation map for MGs in (e) stress–temperature and (f) strain rate–temperature axes. The absolute stress values shown are for the specific glass $Zr_{41.2}Ti_{13.8}Cu_{12.5}Ni_{10}Be_{22.5}$.[138] With permission from Acta Materialia. Copyright 2007 Elsevier.

As the plastic strain is carried by shear bands, understanding their structure is the key to understanding the plasticity of MGs. The formation of shear bands can be well described by a two-stage model.[184] At the first stage, a viable band is created for shearing by structural rejuvenation. The structure in a shear band at the first stage becomes disordered and ready to flow compared with the surrounding matrix. The strain in the first stage is still very small. Right after the formation of first stage, the second stage happens by synchronized sliding and shear-off along the rejuvenated plane. The softening of shear bands may come from two reasons: first, shearing will induce dilatation which lowers the viscosity as discussed above; second, during the operation of shear band, the local temperature will rise above the glass transition temperature to reduce the viscosity. Lewandowski *et al.*[185] demonstrated that the temperature rises after the formation of some shear bands. As shown in Fig. 9(c), the coated tin layer was melted at the shear offset, indicating heat was generated. The catastrophic failure of MGs is attributed to the so-called hot shear bands which cause local heating and melting of the materials inside the shear bands. It was[139,186] further found that there are cold shear bands which are associated with serrated flow and cause the stick-slip sliding behavior. The cold shear bands are responsible for the plasticity of MGs. However, the underlying reason why some shear bands will cause catastrophic failure while others will not is still not clear.

The problem that prevents the wider application of MGs as structural materials is that they always lack strain hardening. Another problem is that to date no MGs have tensile plasticity except for samples in nanometer sizes.[187] Tensile plasticity for bulk samples is only achieved in some partially crystallized MGs.[188,189]

When temperature is close to glass transition temperature and the strain rate is relatively slow, the stress induced free volume will be annihilated quickly by thermal diffusion. In such cases, the plastic deformation is dominated by homogeneous flow. Kawamura reported that when the La–Al–Ni MG was deformed at a temperature above the glass transition temperature, it elongated to 1800% of its original length, showing a superplastic deformation behavior.[190] Lu *et al.*[191] studied the deformation behavior of Zr-based MGs as a function of temperature. Figure 9(d) shows the stress-strain curve at a constant strain rate. At low temperature, the yield strength of a MG is high and the plasticity is low. At high temperature, the yield strength is low and the MG begins to be deformed by a homogeneous flow.

Considering the influence of stress, strain rate, and temperature, a deformation map was first constructed by Spaepen.[148] Later, Schuh *et al.*[138] created a redrawn deformation map which is shown in Figs. 9(e) and 9(f). This deformation map provides a good summary of the overall deformation behavior of MGs. As shown in Fig. 9(e), at low stress and low temperature, the deformation is elastic. When the stress is higher than the yield strength, inhomogeneous flow begins. On the other hand, at low stress and high temperature, homogeneous flow begins and can be further divided into Newtonian flow and non-Newtonian flow. Last, at high stress and high temperatures, inhomogeneous flow dominates again. The deformation behavior is also strongly influenced by shear rate. Figure 9(f) shows when shear rate is faster, the deformation becomes more inhomogeneous.

## 6. Soft-magnetic property of metallic glasses

Soft-magnetic MGs have attracted a great deal of research and industry interest since the first discovery of Fe–P–C MG in the 1970s.[192] Because of the low coercivity, low magnetostriction, and high electrical resistance, soft-magnetic MGs show an advantage in energy saving when used as the cores in electric power distribution transformers and electrical motors. Figure 10(a) shows the magnetic permeability and saturation magnetization of the general soft-magnetic materials.[193] Co-based amorphous alloys have the highest permeability of all, and it is several orders greater than that of the traditional silicon steels. Fe-based amorphous alloys have a high saturation magnetization comparable to the silicon steels. Nanocrystalline Fe-based alloys, which are made from amorphous precursors, show good permeability and saturation magnetization in between the amorphous Co-based alloy and amorphous Fe-based alloy. In the following section, the origin of soft-magnetic property in these materials and the recent development of soft-magnetic MGs and nano-crystalline alloys will be briefly discussed. There are also some good review papers on this topic in Refs. [194] and [195] for readers' interests.

### 6.1. Magnetic structure of soft-magnetic metallic glasses

As indicated by definition, the magnetic moment correlation in soft-magnetic MGs is dominated by ferromagnetic interaction.[196] Because of the random atomic structure, the magnetic moments are not perfectly aligned parallel with each other but rather have some degrees of canting angle, as revealed by neutron diffraction experiments.[197,198] The magnetic structures in the medium range (from several angstroms to tens of nanometers), e.g., magnetic domains and domain walls, were studied by the Small Angle Neutron Scattering (SANS).[199–205] The magnetic domains of soft-magnetic MGs were found to be influenced by fabrication processes, surface defects, and chemical inhomogeneity.

### 6.2. Random anisotropy model

The structure of MGs can be considered random at long range, but with short-to-medium range orders as described in

the above sessions. Because of the absence of crystalline lattices, MGs do not have magneto-crystalline anisotropy. Instead, the magneto anisotropy mainly comes from the nearest neighboring atomic arrangement. The short-to-medium atomic arrangements in MGs vary with location, resulting in local anisotropies with random orientations.

The random anisotropy model (RAM)[206] is applied to explain the magnetic property in the amorphous alloys. Figure 10(b) is a schematic picture of the RAM.[195] For amorphous alloy based on 3d-based late transition metals (Fe, Co, Ni), the local anisotropy $K_1$ is weak, while the magnetic exchange interaction is strong. Thus, on a large scale, the total energy when magnetic moments follow the local easy axis is larger than the total energy when magnetic moments are aligned parallel with each other. The exchange length $L_{ex}$ is then determined by the average anisotropy $\langle K\rangle$, as expressed in the following equation:

$$L_{ex} = \varphi\sqrt{A/\langle K\rangle} = \frac{\varphi^4 A^2}{K^2 D^3}, \tag{1}$$

where $A$ is the exchange stiffness, $K$ is the local magneto anisotropy constant, $\varphi$ is a dimensionless parameter of the order of one, and $D$ is the correlation length describing the scale of anisotropy fluctuation. In metallic glasses, $D$ is usually on the order of one nanometer. Set $A$ to be $10^{-11}$ J/m and $K$ to be $5\times10^4$ J/m$^3$ for a 3d-based amorphous alloy, the exchange length $L_{ex}$ is on the order of 10–100 μm.[207] Figure 10(c) is the Scanning Electron Microscopy with Polarization Analysis (SEMPA) picture of the magnetic moment orientation in a soft-magnetic amorphous alloy.[208] The same color indicates the same direction of magnetic moments. It shows that the exchange length is about 10–100 μm, confirming the validity of the random anisotropy model.

According to RAM, the average anisotropy is described by

$$\langle K\rangle = \frac{K^4}{\varphi^6 A^3} D^6. \tag{2}$$

It scales with $D^6$. However, experiments show that when $D$ becomes smaller than about 10 nm, this law breaks down. This is because other factors should be taken into consideration when calculating the total anisotropy. These factors include surface defects, internal stresses, etc., which induce a weak but long range anisotropy. Usually, the internal stresses determine the coercivity in the as-cast MGs. When MGs are put into isothermal annealing to release the internal stresses, the coercivity will drop.[209] Similarly, MGs with a larger casting thickness also show a smaller coercivity because of less internal stresses.[210,211]

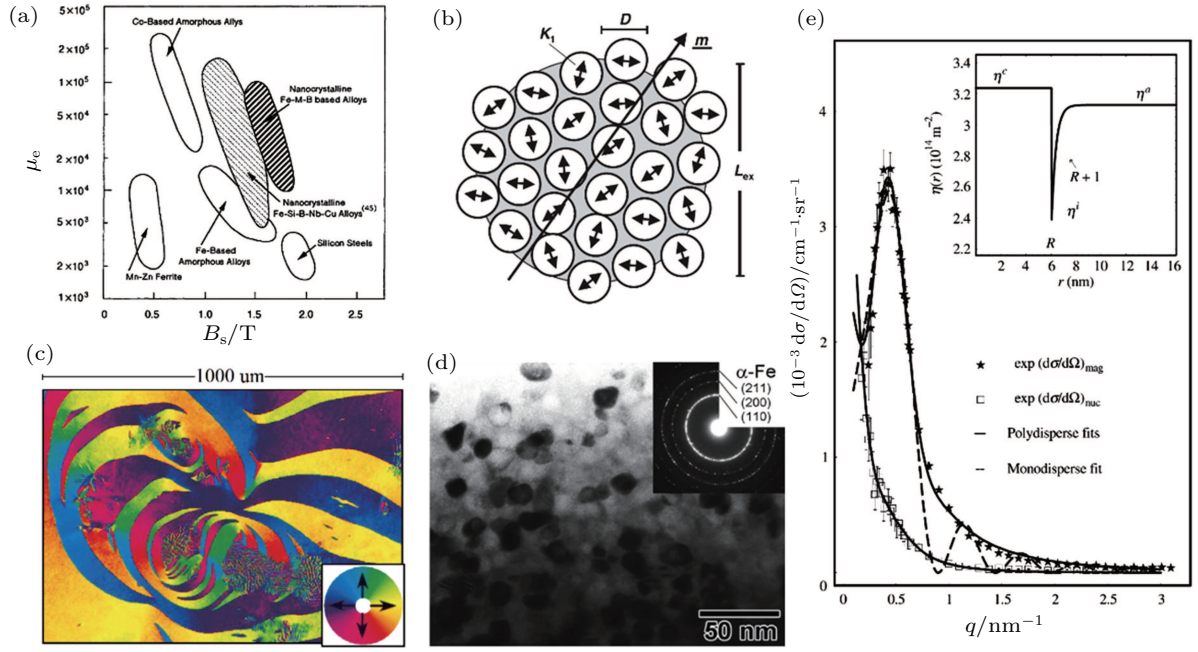



**Fig. 10.** (color online) (a) Relation between $B_s$ and $\mu_e$ at 1 kHz for amorphous Fe and Co based alloys, nano-crystalline Fe–M–B based alloys, nano-crystalline Fe–Si–B–Nb–Cu alloys, Mn–Zn ferrite, and silicon steels.[193] With permission from Materials Transactions. Copyright 1995 the Japan Institute of Metals and Materials. (b) Schematic representation of the random anisotropy model for grains embedded in an ideally soft ferromagnetic matrix. The double arrows indicate the randomly fluctuating anisotropy axis; the hatched area represents the ferromagnetic correlation volume determined from the exchange length $L_{ex}$ within which the orientation $m$ of the magnetization is constant.[195] With permission from Acta Materialia. Copyright 2013 Elsevier. (c) SEMPA image of the magnetization direction (color) and topography from the air side of an as-cast amorphous ribbon. The magnetization direction is color coded to the color wheel in the inset. The ribbon's long axis is horizontal.[208] With permission from Journal of Magnetism and Magnetic Materials. Copyright 2000 Elsevier. (d) Bright field image and SAED patterns of nano-crystalline $Fe_{83.3}Si_4B_8P_4Cu_{0.7}$ alloy.[242] With permission from Materials Transactions. Copyright 2009 The Japan Institute of Metals and Materials. (e) Experimental small-angle neutron scattering data and fits for the $Fe_{73.5}Si_{15.5}B_7CuNb_3$ system with 2 vol.% $Fe_{80}Si_{20}$ precipitates. The inset shows the magnetic scattering length density. $\eta_c$, $\eta_i$, and $\eta_a$, are the magnetic scattering length density of the core, shell, and amorphous matrix, respectively.[248] Reproduced with permission of the International Union of Crystallography.

### 6.3. Recent development of soft-magnetic metallic glasses

Recent years have seen the development of soft-magnetic MGs. Research in this field is targeting soft-magnetic MGs with good GFA, high saturation magnetization, low coercivity, low magnetostriction and good ductility. BMGs with a critical casting thickness larger than 1 mm and good soft-magnetic properties were reported in alloy systems based on 3d-based late transition metals (Fe, Co, Ni).[210,212–233] For example, the Fe–Mo–P–C–B–Si BMG[210] has a critical casting thickness of 4 mm with a good soft-magnetic property ($B_s \sim 1.3$ T and $H_c \sim 1.5$ A/m). The saturation magnetization in Fe–Si–B–P BMG[209] can reach about 1.6 T. On the other hand, in some Fe–B–Nb–Y MGs,[220] the coercivity is as low as 0.35 A/m.

To achieve the best soft-magnetic property, MGs need to be annealed below $T_g$ to release internal stresses. However, the annealing will also induce embrittlement,[234–237] which causes problems during application. An important direction in this field is to develop superior alloy compositions or processing procedures to maintain both good soft-magnetic property and good plasticity.

### 6.4. Nano-crystalline soft-magnetic materials

Nano-crystalline soft-magnetic materials are usually made by crystallization of the amorphous precursors.[238] The grain size is on the order of 10 nm. It was first developed in Fe–Si–B–Nb–Cu alloy system called FINEMET by Yoshizawa *et al.*[239] Soon after that, Suzuki *et al.* developed Fe–Zr–B nano-crystalline alloy which has zero magnetostriction.[240] As described by the RAM, the average anisotropy scales with $D^6$. Thus, the resultant nano-crystalline materials with small grain size show superior soft-magnetic property.[241] In recent years, Makino *et al.* successfully made a new type of nano-crystalline alloy by crystallization of the amorphous Fe–Si–B–P–Cu alloy.[242,243] This new nano-crystalline alloy (called NANOMET) shows a high saturation magnetization ($\sim 1.9$ T), which is comparable with silicon steels and much higher than the FINEMET alloy ($\sim 1.3$ T). Figure 10(d) shows the TEM bight field image of the NANOMET alloy.[242] Finely dispersed $\alpha$-Fe crystals are imbedded in an amorphous matrix. The grain size is small, ensuring this material has an excellent soft-magnetic property.

The mechanism of nano-crystallization in the above systems was studied extensively. For example, it was found the FINEMET alloy shows a finest grain structure with an optimized amount of Cu by the SANS study.[244,245] Using polarized neutron scattering,[246,247] Heinemann *et al.*[248] studied the crystallization of the FINEMET alloy. Figure 10(e) is the experimental SANS data and fits for the $Fe_{73.5}Si_{15.5}B_7CuNb_3$ system with 2% volume fraction of $Fe_{80}Si_{20}$ precipitates. The magnetic scattering and nuclear scattering are separated due to the advantage of polarized neutron scattering. A core-shell structure is found to well describe the crystal structure in this system. The magnetic scattering length density $\eta$, grain size $R$ and the characteristic length of the shell l are then obtained from the fitting of the SANS results and shown in the inset of Fig. 10(e). According to the obtained magnetic scattering length density, the shell is enriched of Nb, which is believed to slow down the crystal growth rate of this system and result in the nano-sized grain structure.

## 7. Summary and outlook

A brief survey is provided on the multiscale structures of metallic glasses. Neutron and synchrotron scattering played an important role in elucidating the complex structures, by breaking down the structures to the fundamental unit level (the short-range order) and the packing or connectivity between the structure units (medium-range order). The response of the structures, the changes at short- and medium-range order levels, determine the properties. An example is shown for mechanical deformation. The magnetic structures are discussed in a similar context.

The rapid development of the next-generation synchrotron and neutron sources and the associated cutting-edge sample environments could provide greater opportunities for study of multiscale structures of metallic glasses. New experiments will be enabled, particularly in the study of dynamic behaviors. For example, using x-ray free electron laser (XFEL), it is possible to capture motion of individual atoms during a phase transformation or a chemical reaction process in a few femtoseconds (1 fs = $10^{-15}$ s),[249] which would be very useful for unraveling the atomic origin of complex phase transformations in multicomponent materials such as metallic glasses. The spallation neutron sources, such as the China Spallation Neutron Source (CSNS),[250] provide high flux which will enable time-resolved measurements of structure evolution in real time. With advanced instrumentation, phonon dynamics in metallic glasses can be examined in detail[251] by inelastic neutron scattering, and in the future, as a function of time. Small angle neutron scattering remains a vital tool for exploring the unusual magnetic structures with hidden order in metallic glasses. Finally, novel scattering sample environments such as beamline electro-static levitator enable direct measurements of structure evolution from liquid state to glass state, i.e., *in situ* vitrification process, using neutron or high energy x-ray scattering techniques.

## References


[1] Iwashita and Inoue A 2000 *Acta Mater.* **48** 279

[2] Johnson W L 2000 In: *Abstracts of Papers of the American Chemical Society* 1155 16th ST, NW, Washington, DC 20036 USA: Amer Chemical Soc, 2000 pp. U282–U282

[3] Wang J Q, Shen Y, Perepezko J H and Ediger M D 2016 *Acta Materialia* **104** 25

[4] Weintraub H, Ashburner M, Goodfellow P N, Lodish H F, Arntzen C J, Anderson P W, Rice T M, Geballe T H, Means A R, Ranney H M, Cech T R, Colwell R R, Bourne H R, Richter B, Singer I M, Marrack P, Fearon D T, Penzias A, Bard A J, Brinkman W F, Marks P A, Vogelstein B, Kinzler K W, Bishop J M, Zare R N, Schatz G, Benkovic S J,

Gray H B, Valentine J S, Crutzen P J, Choi D W, Nakanishi S, Kosslyn S M, Brauman J I, Rees D C, Brill W J, Schell J, Luhrmann R, Will C L, Wulf W, Vermeij G J, Arrow K J, Smelser N J, Anderson D L and Abelson P H 1995 *Science* **267** 1609
[5] Ediger M D, Angell C A and Nagel S R 1996 *J. Phys. Chem.-Us.* **100** 13200
[6] Debenedetti P G and Stillinger F H 2001 *Nature* **410** 259
[7] Zhang C S, Peng M and Sun G A 2015 *Physics* **44** 169
[8] Liu Y T and Chen D F 2013 *Physics* **42** 534
[9] Miracle D B 2013 *Acta Materialia* **61** 3157
[10] Finney J in *Proceedings of the Royal Society of London A: Mathematical, Physical and Engineering Sciences* 479 (The Royal Society).
[11] Bernal J D and Finney J L 1967 *Discussions of the Faraday Society* **43** 62
[12] Tanaka H 2005 *Journal of Non-Crystalline Solids* **351** 678
[13] Hirata A, Kang L J, Fujita T, Klumov B, Matsue K, Kotani M, Yavari A R and Chen M W 2013 *Science* **341** 376
[14] Yavari A R 2006 *Nature* **439** 405
[15] Miracle D B 2004 *Nature Materials* **3** 697
[16] Ma D, Stoica A D, Yang L, Wang X L, Lu Z P, Neuefeind J, Kramer M J, Richardson J W and Proffen T 2007 *Appl. Phys. Lett.* **90** 211908
[17] Kelton K F, Lee G W, Gangopadhyay A K, Hyers R W, Rathz T J, Rogers J R, Robinson M B and Robinson D S 2003 *Phys. Rev. Lett.* **90** 195504
[18] Tarjus G, Kivelson S A, Nussinov Z and Viot P 2005 *J. Phys.-Condens Mat.* **17** R1143
[19] Nelson D R 1983 *Phys. Rev. B* **28** 5515
[20] Cheng Y, Ma E and Sheng H 2009 *Phys. Rev. Lett.* **102** 245501
[21] Ma D, Stoica A D and Wang X L 2009 *Nat. Mater.* **8** 30
[22] Freltoft T, Kjems J K and Sinha S K 1986 *Phys. Rev. B* **33** 269
[23] Zeng Q, Kono Y, Lin Y, Zeng Z, Wang J, Sinogeikin S V, Park C, Meng Y, Yang W and Mao H K 2014 *Phys. Rev. Lett.* **112** 185502
[24] Barmin Y V, Bataronov L L and Bondarev A V 2005 *Nato Sci Ser Ii-Math* **184** 209
[25] Chen D Z, Shi C Y, An Q, Zeng Q S, Mao W L, Goddard W A and Greer J R 2015 *Science* **349** 1306
[26] Kaushik M, Basu K, Benoit C, Cirtiu C M, Vali H and Moores A 2015 *J. Am. Chem. Soc.* **137** 6124
[27] Ruprecht J and Nield J 2001 *Prog Biophys Mol Bio* **75** 121
[28] Das A, Boldt R, Jurk R, Jehnichen D, Fischer D, Stockelhuber K W and Heinrichac G 2014 *Rsc Adv.* **4** 9300
[29] Vahedi-Faridi A, Jastrzebska B, Palczewski K and Engel A 2013 *Microscopy-Jpn* **62** 95
[30] Yang L, Wang X L, Stoica A D, Almer J, Shi D and Wang W H 2008 *Metall. Mater. Trans. A* **39A** 1947
[31] Yang L, Miller M K, Wang X L, Liu C T, Stoica A D, Ma D, Almer J and Shi D 2009 *Adv. Mater.* **21** 305
[32] Wang X L, Almer J, Liu C, Wang Y, Zhao J, Stoica A, Haeffner D and Wang W 2003 *Phys. Rev. Lett.* **91** 265501
[33] Kelton K F and Holzer J C 1988 *Phys. Rev. B* **37** 3940
[34] Huett V T and Kelton K F 2002 *Appl. Phys. Lett.* **81** 1026
[35] Du X and Huang J 2007 *Chin. Phys. Lett.* **24** 1335
[36] Lan S, Yip Y, Lau M and Kui H 2012 *J. Non-Crystalline Solids* **358** 1298
[37] Lan S, Wu Z D, Lau M T and Kui H W 2013 *J. Non-Crystalline Solids* **373-374** 5
[38] Lan S, Wu Z D, Wei X Y, Zhou J, Lu Z P, Wu X L, Neuefeind J and Wang X L 2016 unpublished
[39] Cahn J W and Hilliard J E 1958 *The Journal of chemical physics* **28** 258
[40] Cahn J W and Hilliard J E 1959 *The Journal of chemical physics* **31** 688
[41] Inoue A, Chen S and Masumoto T 1994 *Materials Science and Engineering: A* **179** 346
[42] Matsuura M, Sakurai M, Suzuki K, Chen S and Inoue A 1995 *Physica B: Condensed Matter* **208** 357
[43] Kündig A, Ohnuma M, Ping D, Ohkubo T and Hono K 2004 *Acta Materialia* **52** 2441
[44] Park B, Chang H, Kim D and Kim W 2004 *Appl. Phys. Lett.* **85** 6353
[45] Park B J, Chang H J, Kim D H, Kim W T, Chattopadhyay K, Abinandanan T and Bhattacharyya S 2006 *Phys. Rev. Lett.* **96** 245503
[46] Mattern N, Kühn U, Gebert A, Gemming T, Zinkevich M, Wendrock H and Schultz L 2005 *Scripta Mater* **53** 271
[47] Park E and Kim D 2006 *Acta Materialia* **54** 2597
[48] Park E, Kyeong J and Kim D 2007 *Scripta Mater* **57** 49
[49] Park E, Jeong E, Lee J K, Bae J, Kwon A, Gebert A, Schultz L, Chang H and Kim D 2007 *Scripta Mater* **56** 197
[50] Park B J, Sohn S W, Kim D H, Jeong H T and Kim W T 2008 *J. Mater. Res.* **23** 828
[51] Wada T, Louzguine-Luzgin D V and Inoue A 2007 *Scripta Mater* **57** 901
[52] Chang H, Yook W, Park E, Kyeong J and Kim D 2010 *Acta Materialia* **58** 2483
[53] Han J, Mattern N, Kim D and Eckert J 2011 *J. Alloy Compd.* **509** S42
[54] Han J, Mattern N, Schwarz B, Kim D and Eckert J 2012 *Scripta Mater* **67** 149
[55] Sohn S, Yook W, Kim W and Kim D 2012 *Intermetallics* **23** 57
[56] Park J M, Han J H, Mattern N, Kim D H and Eckert J 2012 *Metallurgical and Materials Transactions A* **43** 2598
[57] Chen S, Tu J, Wu J, Hu Q, Xie S, Zou J and Zeng X 2016 *Materials Science and Engineering: A* **656** 84
[58] Chen H and Turnbull D 1969 *Acta Metallurgica* **17** 1021
[59] Chou C P and Spaepen F 1975 *Acta Metallurgica* **23** 609
[60] Chen H 1976 *Mater Sci Eng* **23** 151
[61] Leung C, Guo W and Kui H 2000 *Appl.Phys. Lett.* **77** 64
[62] Wu Z D, Zhou W Z, Lo Y F, Lan S and Kui H W 2015 *Journal of Non-Crystalline Solids* **410** 51
[63] Zhou W, Wu Z, Lo Y and Kui H 2016 *Journal of Non-Crystalline Solids* **432** 420
[64] Tanner L E and Ray R 1980 *Scripta Metall Mater* **14** 657
[65] Hays C, Kim C and Johnson W 1999 *Appl. Phys. Lett.* **75** 1089
[66] Hufnagel T C, Gu X and Munkholm A 2001 *Materials Transactions* **42** 562
[67] Wang W H, Wei Q and Friedrich S 2000 *J. Mater. Sci.* **35** 2291
[68] Lffler J F and Johnson W L 2000 *Appl. Phys. Lett.* **76** 3394
[69] Pelletier J M and Van de Moortèle B 2003 *Journal of Non-crystalline Solids* **325** 133
[70] Martin I, Ohkubo T, Ohnuma M, Deconihout B and Hono K 2004 *Acta Materialia* **52** 4427
[71] Yavari A, Hamar-Thibault S and Sinning H 1988 *Scripta Metall Mater* **22** 1231
[72] Yavari A, Osamura K, Okuda H and Amemia Y 1988 *Phys. Rev. B* **37** 7759
[73] Madge S, Rsner H and Wilde G 2005 *Scripta Mater* **53** 1147
[74] Lau M T, Lan S, Yip Y L and Kui H W 2012 *Journal of Non-Crystalline Solids* **358** 2667
[75] Lan S, Lau M T and Kui H W 2013 *Journal of Non-Crystalline Solids* **361** 1
[76] Wu Z, Lu X, Wu Z and Kui H 2014 *Journal of Non-Crystalline Solids* **385** 40
[77] Lu K and Wang J 1989 *J Cryst Growth* **94** 448
[78] Yu H B, Wang W H, Bai H Y and Samwer K 2014 *National Science Review* **1** 429
[79] Spaepen F 2006 *Scripta Mater* **54** 363
[80] Heggen M, Spaepen F and Feuerbacher M 2005 *Journal of Applied Physics* **97** 33506
[81] Spaepen F. Defects in Amorphous Metals. (DTIC Document, 1982).
[82] Hai-Lian H, Chuang D, Qing W, Yu Z and Yao-Xiang G 2016 *Acta Phys. Sin.* **65** (in Chinese)
[83] Sheng H W, Luo W K, Alamgir F M, Bai J M and Ma E 2006 *Nature* **439** 419
[84] Kündig A, Ohnuma M, Ohkubo T and Hono K 2005 *Acta Materialia* **53** 2091
[85] Shen Y T, Kim T H, Gangopadhyay A K and Kelton K F 2009 *Phys. Rev. Lett.* **102** 057801
[86] Lee G W, Gangopadhyay A K, Croat T K, Rathz T J, Hyers R W, Rogers J R and Kelton K F 2005 *Phys. Rev. B* **72** 174107
[87] Pekarskaya E, Lffler J F and Johnson W L 2003 *Acta Materialia* **51** 4045
[88] Yang C M, Bian F G, Xiong B Q, Liu D M, Li Y W, Hua W Q and Wang J 2016 *Chin. Phys. B* **25** 066101
[89] Tang C and Harrowell P 2013 *Nat. Mater.* **12** 507
[90] Lan S, Wei X Y, Zhou J, Lu Z P, Wu X L, Feygenson M, Neuefeind J and Wang X L 2014 *Appl. Phys. Lett.* **105** 201906

[91] Sanz E, Valeriani C, Zaccarelli E, Poon W C K, Cates M E and Pusey P N 2014 *Proceedings of the National Academy of Sciences of the United States of America* **111** 75
[92] Tanaka H 2000 *Phys. Rev. E* **62** 6968
[93] Poole P H, Sciortino F, Essmann U and Stanley H E 1992 *Nature* **360** 324
[94] Katayama Y, Mizutani T, Utsumi W, Shimomura O, Yamakata M and Funakoshi K I 2000 *Nature* **403** 170
[95] van Thiel M and Ree F 1993 *Phys. Rev. B* **48** 3591
[96] Sastry S and Austen Angell C 2003 *Nat. Mater.* **2** 739
[97] Poole P H, Hemmati M and Angell C A 1997 *Phys. Rev. Lett.* **79** 2281
[98] Barkalov O I, Tissen V G, McMillan P F, Wilson M, Sella A and Nefedova M V 2010 *Phys. Rev. B* **82** 020507
[99] Bhat M, Molinero V, Soignard E, Solomon V, Sastry S, Yarger J and Angell C 2007 *Nature* **448** 787
[100] Lacks D J 2000 *Phys. Rev. Lett.* **84** 4629
[101] Harrington S, Zhang R, Poole P H, Sciortino F and Stanley H E 1997 *Phys. Rev. Lett.* **78** 2409
[102] Soper A K and Ricci M A 2000 *Phys. Rev. Lett.* **84** 2881
[103] Palmer J C, Martelli F, Liu Y, Car R, Panagiotopoulos A Z and Debenedetti P G 2014 *Nature* **510** 385
[104] Nilsson A and Pettersson L G 2015 *Nat. Commun.* **6** 8998
[105] Aasland S and Mcmillan P F 1994 *Nature* **369** 633
[106] Shimizu R, Kobayashi M and Tanaka H 2014 *Phys. Rev. Lett.* **112** 125702
[107] Tanaka H, Kurita R and Mataki H 2004 *Phys. Rev. Lett.* **92** 025701
[108] Xu L, Kumar P, Buldyrev S V, Chen S H, Poole P H, Sciortino F and Stanley H E 2005 *Proceedings of the National Academy of Sciences of the United States of America* **102** 16558
[109] Xu L, Mallamace F, Yan Z, Starr F W, Buldyrev S V and Stanley H E 2009 *Nat. Phys.* **5** 565
[110] Xu L, Buldyrev S V, Angell C A and Stanley H E 2006 *Phys. Rev. E* **74** 031108
[111] Kim T H, Goldman A I and Kelton K F 2008 *Philos. Mag.* **88** 171
[112] Angell C, Bressel R, Hemmati M, Sare E and Tucker J 2000 *Phys. Chem. Chem. Phys.* **2** 1559
[113] Du J, Benmore C J, Corrales R, Hart R T and Weber J R 2009 *Journal of Physics: Condensed Matter* **21** 205102
[114] Hédoux A, Derollez P, Guinet Y, Dianoux A J and Descamps M 2001 *Phys. Rev. B* **63** 144202
[115] Tanaka H 2005 *Journal of Non-crystalline Solids* **351** 3385
[116] Tanaka H 2005 *Journal of Non-crystalline Solids* **351** 3371
[117] Tanaka H 1999 *Journal of Physics: Condensed Matter* **11** L159
[118] Tanaka H 1999 *Journal of Chemical Physics* **111** 3163
[119] Tanaka H 1999 *Journal of Chemical Physics* **111** 3175
[120] Biroli G and Bouchaud J-P 2012 *Structural Glasses and Supercooled Liquids: Theory, Experiment, and Applications* 31
[121] Tanaka H 1998 *Phys. Rev. Lett.* **80** 5750
[122] Adam G and Gibbons G J 1965 *The Journal of Chemical Physics* **43** 139
[123] Sheng H W, Liu H Z, Cheng Y Q, Wen J, Lee P L, Luo W K, Shastri S D and Ma E 2007 *Nat. Mater.* **6** 192
[124] Zeng Q S, Ding Y, Mao W L, Yang W, Sinogeikin S V, Shu J, Mao H K and Jiang J Z 2010 *Phys. Rev. Lett.* **104** 105702
[125] Ito K, Moynihan C T and Angell C A 1999 *Nature* **398** 492
[126] Zhang C, Hu L, Yue Y and Mauro J C 2010 *The Journal of Chemical Physics* **133** 014508
[127] Elmatad Y S 2011 *Proceedings of the National Academy of Sciences of the United States of America* **108** E230; author reply E231
[128] Evenson Z, Schmitt T, Nicola M, Gallino I and Busch R 2012 *Acta Materialia* **60** 4712
[129] Sun Q, Zhou C, Yue Y and Hu L 2014 *Journal of Physical Chemistry Letters* **5** 1170
[130] Yang X N, Zhou C, Sun Q J, Hu L N, Mauro J C, Wang C Z and Yue Y Z 2014 *J Phys Chem B* **118** 10258
[131] Li J J Z, Rhim W K, Kim C P, Samwer K and Johnson W L 2011 *Acta Materialia* **59** 2166
[132] Wei S, Yang F, Bednarcik J, Kaban I, Shuleshova O, Meyer A and Busch R 2013 *Nat. Commun.* **4** 2083
[133] Georgarakis K, Hennet L, Evangelakis G, Antonowicz J, Bokas G, Honkimaki V, Bytchkov A, Chen M and Yavari A 2015 *Acta Materialia* **87** 174
[134] Xu W, Sandor M T, Yu Y, Ke H B, Zhang H P, Li M Z, Wang W H, Liu L and Wu Y 2015 *Nat. Commun.* **6** 7969
[135] Lan S, Blodgett M, Kelton K F, Ma J L, Fan J and Wang X L 2016 *Appl. Phys. Lett.* **108** 211907
[136] Wessels V, Gangopadhyay A K, Sahu K K, Hyers R W, Canepari S M, Rogers J R, Kramer M J, Goldman A I, Robinson D, Lee J W, Morris J R and Kelton K F 2011 *Phys. Rev. B* **83** 094116
[137] Wang W H 2012 *Progress in Materials Science* **57** 487
[138] Schuh C A, Hufnagel T C and Ramamurty U 2007 *Acta Materialia* **55** 4067
[139] Trexler M M and Thadhani N N 2010 *Progress in Materials Science* **55** 759
[140] Greer A, Cheng Y and Ma E 2013 *Materials Science and Engineering: R: Reports* **74** 71
[141] Ashby M and Greer A 2006 *Scripta Materialia* **54** 321
[142] Dmowski W, Iwashita T, Chuang C P, Almer J and Egami T 2010 *Phys. Rev. Lett.* **105** 205502
[143] Egami T, Tong Y and Dmowski W 2016 *Metals* **6** 22
[144] Künzi H U 1983 in *Glassy Metal II* 169 (Springer)
[145] Li Y, Guo Q, Kalb J and Thompson C 2008 *Science* **322** 1816
[146] Ma D, Stoica A D, Wang X L, Lu Z P, Clausen B and Brown D W 2012 *Phys. Rev. Lett.* **108** 085501
[147] Polk D and Turnbull D 1972 *Acta Metallurgica* **20** 493
[148] Spaepen F 1977 *Acta Metallurgica* **25** 407
[149] Argon A 1979 *Acta Metallurgica* **27** 47
[150] An Q, Samwer K, Demetriou M D, Floyd M C, Duggins D O, Johnson W L and Goddard W A 2016 *Proceedings of the National Academy of Sciences* **113** 7053
[151] Demetriou M D, Launey M E, Garrett G, Schramm J P, Hofmann D C, Johnson W L and Ritchie R O 2011 *Nat. Mater.* **10** 123
[152] Schroers J and Johnson W L 2004 *Phys. Rev. Lett.* **93** 255506
[153] Yao K, Ruan F, Yang Y and Chen N 2006 *Appl. Phys. Lett.* **88** 122106
[154] Granata D, Fischer E, Wessels V and Lffler J F 2014 *Acta Materialia* **71** 145
[155] Liu L, Pang S, Ma C and Zhang T 2005 *Materials Transactions* **46** 2945
[156] Zhu Z, Zhang H, Sun W, Ding B and Hu Z 2006 *Scripta Materialia* **54** 1145
[157] Das J, Tang M B, Kim K B, Theissmann R, Baier F, Wang W H and Eckert J 2005 *Phys. Rev. Lett.* **94** 205501
[158] Tan J, Zhang Y, Stoica M, Kühn U, Mattern N, Pan F and Eckert J 2011 *Intermetallics* **19** 567
[159] Pan J, Liu L and Chan K 2009 *Scripta Materialia* **60** 822
[160] Jiang Q, Wang X, Nie X, Zhang G, Ma H, Fecht H J, Bendnarcik J, Franz H, Liu Y and Cao Q 2008 *Acta Materialia* **56** 1785
[161] Sun B, Yu H, Jiao W, Bai H, Zhao D and Wang W 2010 *Phys. Rev. Lett.* **105** 035501
[162] Chen L, Fu Z, Zhang G, Hao X, Jiang Q, Wang X, Cao Q, Franz H, Liu Y and Xie H 2008 *Phys. Rev. Lett.* **100** 075501
[163] Mondal K, Ohkubo T, Mukai T and Hono K 2007 *Materials Transactions* **48** 1322
[164] Dan W, Min-Hua S, Li-Feng F, Qiang Z, Li-Juan X, Jia L and Wen-Bin B 2008 *Chin. Phys. Lett.* **25** 2596
[165] Zhu Z, Zhang H, Pan D, Sun W and Hu Z 2006 *Advanced Engineering Materials* **8** 953
[166] Wang K, Fujita T, Zeng Y, Nishiyama N, Inoue A and Chen M 2008 *Acta Materialia* **56** 2834
[167] Liu Y, Wang G, Pan M, Yu P, Zhao D and Wang W 2007 *Journal of Materials Research* **22** 869
[168] Lee M, Lee J, Bae D, Kim W, Sordelet D and Kim D 2004 *Intermetallics* **12** 1133
[169] Jia P, Guo H, Li Y, Xu J and Ma E 2006 *Scripta Materialia* **54** 2165
[170] Kim Y, Lee J, Cha P, Ahn J and Fleury E 2006 *Materials Science and Engineering: A* **437** 248
[171] Zhang T, Liu F, Pang S and Li R 2007 *Materials Transactions* **48** 1157
[172] Yao K and Zhang C 2007 *Appl. Phys. Lett.* **90** 061901
[173] Dun C, Liu H, Hou L, Xue L, Dou L, Yang W, Zhao Y and Shen B 2014 *Journal of Non-Crystalline Solids* **386** 121
[174] Park E, Chang H and Kim D 2007 *Journal of Materials Research* **22** 334
[175] Hao G, Lin J, Zhang Y J, Chen G and Lu Z 2010 *Materials Science and Engineering: A* **527** 6248

[176] Wang Y L and Xu J 2008 *Metall and Mat Trans A* **39** 2990
[177] Gong P, Yao K and Shao Y 2012 *Journal of Alloys and Compounds* **536** 26
[178] Wang G, Liu Y, Yu P, Zhao D, Pan M and Wang W 2006 *Appl. Phys. Lett.* **89** 251909
[179] Park J, Chang H, Han K, Kim W and Kim D 2005 *Scripta Materialia* **53** 1
[180] Gong P, Yao K and Shao Y 2012 *Journal of Non-Crystalline Solids* **358** 2620
[181] Zhang L, Shi L L and Xu J 2009 *Journal of Non-Crystalline Solids* **355** 1005
[182] Liu Y H, Wang G, Wang R J, Zhao D Q, Pan M X and Wang W H 2007 *Science* **315** 1385
[183] Wu Z 2015 (PhD thesis: The Chinese University of Hong Kong)
[184] Cao A, Cheng Y and Ma E 2009 *Acta Materialia* **57** 5146
[185] Lewandowski J J and Greer A L 2006 *Nat. Mater.* **5** 15
[186] Cheng Y, Han Z, Li Y and Ma E 2009 *Phys. Rev. B* **80** 134115
[187] Guo H, Yan P F, Wang Y B, Tan J, Zhang Z F, Sui M L and Ma E 2007 *Nat. Mater.* **6** 735
[188] Hofmann D C, Suh J Y, Wiest A, Duan G, Lind M L, Demetriou M D and Johnson W L 2008 *Nature* **451** 1085
[189] Pauly S, Gorantla S, Wang G, Kühn U and Eckert J 2010 *Nat. Mater.* **9** 473
[190] Kawamura Y, Nakamura T, Inoue A and Masumoto T 1999 *Materials Transactions, JIM* **40** 794
[191] Lu J, Ravichandran G and Johnson W L 2003 *Acta Materialia* **51** 3429
[192] Rastogi P and Duwez P 1970 *Journal of Non-Crystalline Solids* **5** 1
[193] Makino A, Inoue A and Masumoto T 1995 *Materials Transactions, JIM* **36** 924
[194] Suryanarayana C and Inoue A 2013 *International Materials Reviews* **58** 131
[195] Herzer G 2013 *Acta Materialia* **61** 718
[196] Coey J 1978 *Journal of Applied Physics* **49** 1646
[197] Wildes A, Cowley R, Al-Heniti S, Cowlam N, Kulda J and Lelièvre-Berna E 1998 *Journal of Physics: Condensed Matter* **10** 2617
[198] Cowley R, Patterson C, Cowlam N, Ivison P, Martinez J and Cussen L 1991 *Journal of Physics: Condensed Matter* **3** 9521
[199] Oleszak D and Milczarek J 1992 *Journal of Materials Science Letters* **11** 302
[200] Yavari R, Desre P and Chieux P 1986 in *Atomic Transport and Defects in Metals by Neutron Scattering,* p. 42 (Springer)
[201] Janot C and George B 1985 *Journal de Physique Lettres* **46** 85
[202] Fish G and Child H 1981 *Journal of Applied Physics* **52** 1880
[203] Cser L, Kovács I, Lovas A, Sváb E and Zsigmond G 1982 *Nuclear Instruments and Methods in Physics Research* **199** 301
[204] Calvo-Dahlborg M, Dahlborg U, Huler F, Tabachnikova E and Bengus V 2002 *Applied Physics A* **74** s1131
[205] Dahlborg U and Calvo-Dahlborg M 2000 *Materials Science and Engineering: A* **283** 153
[206] Alben R, Becker J and Chi M 1978 *Journal of Applied Physics* **49** 1653
[207] O'handley R C 2000 *Modern Magnetic Materials* (Wiley)
[208] Gavrin A and Unguris J 2000 *Journal of Magnetism and Magnetic Materials* **213** 95
[209] Makino A, Kubota T, Chang C, Makabe M and Inoue A 2007 *Materials Transactions* **48** 3024
[210] Shen B, Akiba M and Inoue A 2006 *Applied Physics Letters* **88** 131907
[211] Inoue A and Shen B 2002 *Materials Transactions* **43** 766
[212] Dou L, Liu H, Hou L, Xue L, Yang W, Zhao Y, Chang C and Shen B 2014 *Journal of Magnetism and Magnetic Materials* **358** 23
[213] Makino A, Chang C, Kubota T and Inoue A 2009 *Journal of Alloys and Compounds* **483** 616
[214] Makino A, Kubota T, Makabe M, Chang C and Inoue A 2008 *Materials Science and Engineering: B* **148** 166
[215] Makino A, Kubota T, Chang C, Makabe M and Inoue A 2008 *Journal of Materials Research* **23** 1339
[216] Makino A, Kubota T, Chang C, Makabe M and Inoue A 2008 *Journal of Magnetism and Magnetic Materials* **320** 2499
[217] Zhang J, Chang C, Wang A and Shen B 2012 *Journal of Non-Crystalline Solids* **358** 1443
[218] Li X, Kato H, Yubuta K, Makino A and Inoue A 2010 *Materials Science and Engineering: A* **527** 2598
[219] Kim D H, Park J M, Kim D H and Kim W T 2007 *Journal of Materials Research* **22** 471
[220] Lee S, Kato H, Kubota T, Yubuta K, Makino A and Inoue A 2008 *Materials Transactions* **49** 506
[221] Long Z, Shao Y, Xu F, Wei H, Zhang Z, Zhang P and Su X 2009 *Materials Science and Engineering: B* **164** 1
[222] Huang X, Chang C, Chang Z, Inoue A and Jiang J 2010 *Materials Science and Engineering: A* **527** 1952
[223] Wang J, Li R, Hua N, Huang L and Zhang T 2011 *Scripta Materialia* **65** 536
[224] Shen B and Inoue A 2002 *Materials Transactions* **43** 1235
[225] Shen B, Koshiba H, Kimura H and Inoue A 2000 *Materials Transactions, JIM* **41** 1478
[226] Li Q, Li J, Gong P, Yao K, Gao J and Li H 2012 *Intermetallics* **26** 62
[227] Yang X, Ma X, Li Q and Guo S 2013 *Journal of Alloys and Compounds* **554** 446
[228] Inoue A, Shen B, Koshiba H, Kato H and Yavari A R 2003 *Nat. Mater.* **2** 661
[229] Inoue A, Shen B, Koshiba H, Kato H and Yavari A 2004 *Acta Materialia* **52** 1631
[230] Inoue A, Shen B and Chang C 2006 *Intermetallics* **14** 936
[231] Shen B, Chang C and Inoue A 2007 *Intermetallics* **15** 9
[232] Shen B, Koshiba H, Inoue A, Kimura H and Mizushima T 2001 *Materials Transactions* **42** 2136
[233] Amiya K, Urata A, Nishiyama N and Inoue A 2007 *Journal of Applied Physics* **101** 09N112
[234] Murali P and Ramamurty U 2005 *Acta Materialia* **53** 1467
[235] Chen H 1977 *Scripta Metallurgica* **11** 367
[236] Lewandowski J, Wang W and Greer A 2005 *Philosophical Magazine Letters* **85** 77
[237] Wu T W and Spaepen F 1990 *Philosophical Magazine B* **61** 739
[238] Gleiter H 1991 in *Advanced Structural and Functional Materials,* p. 1 (Springer)
[239] Yoshizawa Y, Oguma S and Yamauchi K 1988 *Journal of Applied Physics* **64** 6044
[240] Suzuki K, Kataoka N, Inoue A, Makino A and Masumoto T 1990 *Materials Transactions, JIM* **31** 743
[241] Herzer G 1990 *IEEE Transactions on Magnetics* **26** 1397
[242] Makino A, Men H, Kubota T, Yubuta K and Inoue A 2009 *Materials Transactions* **50** 204
[243] Makino A, Men H, Kubota T, Yubuta K and Inoue A 2009 *Journal of Applied Physics* **105** 07A308
[244] Ohnuma M, Hono K, Linderoth S, Pedersen J, Yoshizawa Y and Onodera H 2000 *Acta materialia* **48** 4783
[245] Ohnuma M, Suzuki J, Funahashi S, Ishigaki T, Kuwano H and Hamaguchi Y 1995 *Materials Transactions, JIM* **36** 918
[246] Wiedenmann A 2000 *Journal of Applied Crystallography* **33** 428
[247] Wiedenmann A 2001 *Physica B: Condensed Matter* **297** 226
[248] Heinemann A, Hermann H, Wiedenmann A, Mattern N and Wetzig K 2000 *Journal of Applied Crystallography* **33** 1386
[249] McNeil B W and Thompson N R 2010 *Nature Photonics* **4** 814
[250] Chen H and Wang X L 2016 *Nat. Mater.* **15** 689
[251] Abernathy D L, Stone M B, Loguillo M, Lucas M, Delaire O, Tang X, Lin J and Fultz B 2012 *Review of Scientific Instruments* **83** 015114